Packet-Level Throughput Analysis and Energy Efficiency Optimization for UAV-Assisted IAB Heterogeneous Cellular Networks

Yue Zhang, Hangguan Shan, *Senior Member, IEEE*, Meiyan Song, Howard H. Yang, *Member, IEEE*, Xuemin Shen, *Fellow, IEEE*, Qi Zhang, and Xianhua He

***Abstract*—In this paper, we investigate the packet-level throughput and energy efficiency of millimeter-wave unmanned aerial vehicle (UAV)-assisted integrated access and backhaul (IAB) heterogeneous cellular networks with spatiotemporal traffic. Specifically, we develop a theoretical framework to analyze the mean packet throughput and energy efficiency of the network based on stochastic geometry and queueing theory, whereby the spatial randomness of network deployment and the temporal randomness of network traffic can be appropriately characterized. Different from the traditional network performance metrics emphasizing transmission and resource consumption, the packet-level performance helps to better understand the impact of not only packet transmission but also packet waiting time in a multihop network. Simulation results demonstrate that the assistance of IAB-based UAVs can efficiently relieve the load of terrestrial macro- and small-cell networks, and the appropriate network deployment parameters play pivotal roles in improving both the packet-level throughput and energy efficiency performance. By jointly optimizing the key network parameters, the packet energy efficiency can be significantly improved while ensuring the required mean packet throughput of the network.**

***Index Terms*—UAV-assisted heterogeneous network, integrated access and backhaul, spatiotemporal traffic, mean packet throughput, packet energy efficiency.**

I. Introduction

THE millimeter-wave (mmWave) frequency band was introduced to fifth-generation (5G) and beyond communication networks to cope with the extremely scarce spectrum, while the severe attenuation in the mmWave band owing to small wavelengths and high absorption requires the ultradense deployment of small base stations (SBSs) to enhance the coverage [2], [3]. However, it is neither cost-effective nor practical to deploy a large number of fixed SBSs to achieve ubiquitous coverage, especially in rural areas, and take into account the random spatiotemporal variation in network traffic. On the other hand, with the advantages of maneuverability, flexibility, and cost-effectiveness, unmanned aerial vehicles (UAVs) are playing an increasingly important role as aerial access points (APs) to assist ground macro base stations (MBSs) to relieve the network burden in traffic hot-spot areas [4], [5] or recover the communication in time in disaster areas [6]. By establishing line-of-sight (LoS) communication links from high altitude, they can provide a better quality of service for ground user equipment (GUE) whenever and wherever in need [7], [8]. Thus, substituting UAVs for some SBSs is an economical and flexible way to enhance the mmWave network coverage while decreasing the density of SBSs.

Due to the aerial nature of UAVs and the high deployment cost for fiber backhaul of SBSs, wireless backhaul is of considerable importance for UAVs and SBSs to connect to MBSs and influences the service capability that UAVs and SBSs can provide to GUEs. With their very large available bandwidth and large-scale directional antenna arrays, wireless backhaul links over the mmWave band can achieve fiberlike transmission performance [9]. Thereby, integrated access and backhaul (IAB) has been promoted by the 3 rd Generation Partnership Project (3GPP) to support MBSs in providing access and backhaul service in the same mmWave band [10]. Several works have studied the performance of mmWave IAB-enabled SBS-assisted [11], [12] or UAV-assisted [13], [14] cellular networks. However, it was found that spectrum sharing between access and backhaul leads to more complex mutual interference and performance bottlenecks, especially for heterogeneous networks. Additionally, to the best of the authors' knowledge, there exists no research on mmWave IAB heterogeneous cellular networks where UAVs and SBSs collaborate to assist terrestrial MBSs together.

Manuscript received 10 October 2022; revised 12 January 2023; accepted 20 February 2023. Date of publication 3 March 2023; date of current version 18 July 2023. This work was supported in part by the National Natural Science Foundation Program of China (NSFC) under Grants U21A20456 and U21B2029, and in part by the Nokia Donation Project. A preliminary version of this paper appeared in Proc. IEEE Wireless Communications and Networking Conference (WCNC) 2022 [1]. The review of this article was coordinated by Dr. Sudip Misra. *(Corresponding authors: Qi Zhang; Hangguan Shan.)*

Yue Zhang, Hangguan Shan, and Meiyan Song are with the College of Information Science and Electronic Engineering, Zhejiang University, Hangzhou 310027, China (e-mail: zhangyuezy@zju.edu.cn; hshan@zju.edu.cn; songmy@zju.edu.cn).

Howard H. Yang is with the Zhejiang University/University of Illinois at Urbana-Champaign Institute, Zhejiang University, Haining 314400, China (e-mail: haoyang@intl.zju.edu.cn).

Xuemin Shen is with the Department of Electrical and Computer Engineering, University of Waterloo, Waterloo, ON N2L 3G1, Canada (e-mail: sshen@uwaterloo.ca).

Qi Zhang and Xianhua He are with the Nokia Solutions and Networks System Technology (Beijing) Co., Ltd, Hangzhou 310053, China (e-mail: qi.zhang@nokia-sbell.com; xianhua.he@nokia-sbell.com).

Digital Object Identifier 10.1109/TVT.2023.3252093

On the other hand, the ultradense deployment of SBSs will sharply increase energy consumption. Therefore, improving the energy efficiency for a green 5G mobile network has gained tremendous attention [15], [16]. Although exploiting UAVs is promising to decrease the density of ground SBSs and flexibly satisfy the spatiotemporal variation of network traffic, they cost extra communication-unrelated energy to hover in the air with limited battery capacity. Correspondingly, enhancing energy efficiency for UAV-assisted heterogeneous cellular networks becomes a key issue to take full advantage of UAVs and realize energy-efficient green communications [17]. However, to characterize the energy efficiency of heterogeneous networks, the service process of a tandem queue for both access and backhaul links should be considered. As such, new measurement approaches are required to take into account not only packet transmission but also packet queueing in multihop property networks.

Introducing UAVs to traditional terrestrial networks brings both design flexibility and challenges. In this paper, we focus on the following problems:

- How can a mmWave IAB heterogeneous network be designed in which SBSs and UAVs coexist with MBSs to serve spatiotemporal traffic and connect to them for backhaul?
- How can the network performance be modeled by taking into account both the serving processes of access and backhaul and fine tuning the network parameters to improve energy efficiency while achieving satisfactory throughput performance?

In response to these questions, in this paper, we focus on designing and studying the network performance of a mmWave UAV-assisted heterogeneous cellular network, where UAVs and SBSs coexist to assist MBSs with IAB technology for access and backhaul. Specifically, we consider that GUEs can establish access links with MBSs, UAVs, or SBSs, and MBSs can provide backhaul service for UAVs and SBSs. Both access and backhaul links are operated in the same mmWave band. The orthogonal spectrum partition is adopted to reduce the interference between access and backhaul, while to increase spectrum utilization, the access bandwidth is reused by MBSs, UAVs, and SBSs. To improve the network performance, we consider that the UAV height, the density and deployment proportion of UAVs/SBSs, and the spectrum partition between the access and backhaul links can be configured. To capture the impact of the tandem queueing process consisting of both the access and backhaul links on the throughput and energy efficiency, we analyze the network performance from the packet-level point of view and derive analytical expressions for the mean packet throughput (MPT) and packet energy efficiency (PEE) by jointly utilizing stochastic geometry and queueing theory. Our analysis captures the effects of key network features in three domains: the spatial domain in terms of the spatial density and randomness of the locations of APs and GUEs; the temporal domain in terms of random packet arrivals, time-varying waiting and transmission delays; and the link domain in terms of channel contention and link quality. The main contributions of this paper are summarized as follows:

- To accommodate the ever-increasing spatiotemporal traffic in a cost-effective way, we propose mmWave-based UAV-assisted IAB heterogeneous cellular networks by utilizing mmWave's bandwidth advantage for both access and backhaul and UAVs' flexibility to assist terrestrial macro- and small-cell networks for ubiquitous coverage.
- Based on stochastic geometry and queueing theory, a theoretical framework is proposed to characterize the network's performance from the packet-level point of view. Both MPT and PEE are derived. Thus, not only the impact of transmissions over access and backhaul links but also that of queueing delay in the tandem queues, dependent on spatiotemporal network traffic, are studied.
- Based on the proposed theoretical framework, we investigate the impacts of various network parameters on the MPT and PEE performance. Furthermore, we establish an optimization problem to improve the PEE performance while guaranteeing the MPT requirement via alternating optimization with respect to key network configuration parameters.

The rest of this paper is organized as follows. An overview of the related works is given in Section II. In Section III, we describe the system model of the mmWave UAV-assisted IAB heterogeneous cellular network. In Section IV, we develop the theoretical framework for the MPT and PEE and study the network performance optimization problem. Numerical and simulation results are given and discussed in Section V. Finally, we conclude the paper in Section VI.

II. Related Work

In UAV-assisted heterogeneous cellular networks, UAVs can be used as aerial APs to enhance the coverage, capacity, reliability, and energy efficiency of terrestrial cellular networks [18]. The UAVs in [13] are utilized as aerial relay nodes to assist the dynamic backhaul link rerouting in the mmWave macrocells and vehicle-cells coexistence heterogeneous network to improve the network reliability. A UAV-assisted heterogeneous cellular solution was proposed in [19] to deploy UAV-based floating relay cells inside the ground macrocell for dynamic and adaptive coverage enhancement, where the backhaul resource allocation between UAVs and MBSs was analyzed. The UAV coverage radius and system energy efficiency were optimized for the multiband heterogeneous network, where MBSs, SBSs, and UAVs working as aerial APs coexist, with MBSs and UAVs working on the resource-limited microwave band [20]. However, without the analysis of the temporal randomness of network traffic, the previous works only investigated network-level performance metrics under saturated traffic assumption.

From the perspective of packet-level analysis, the user packet throughput defined in [21] characterizes the effect of random packet arrival but without including the packet waiting delay in the buffer. The authors in [22] optimized the scheduling strategy to maximize the MPT of different types of devices under different delay constraints, where the MPT captures the effects

of both queueing and transmission delays. By incorporating the spatial and temporal fluctuations of traffic, several works adopt the MPT as the primary indicator to analyze the performance of heterogeneous and small cell networks based on stochastic geometry and queueing theory [23], [24], [25]. Nevertheless, the above analyses of MPT are all based on the queue status of one-hop access transmission links, and no tandem queues from backhaul to access transmissions are taken into account.

The enhancement of energy efficiency in mmWave heterogeneous networks or UAV-assisted networks has been shown to be attractive in recent research due to the rising energy cost and the pursuit of green 5G networks. The energy efficiency, defined as the total bits of information successfully sent to users by UAVs divided by the total transmit and propulsion energy consumption of UAVs in the area, was maximized in [26] by optimizing the UAV trajectory and user scheduling. The authors in [27] jointly considered the throughput of UAV-user pairs, total system throughput, and energy efficiency of UAV-assisted Internet of Things networks to achieve multiobjective optimization. In addition, the pivotal tradeoff between energy efficiency and network throughput is elaborated in many works, such as relaxing the throughput constraints to maximize the network energy efficiency in mmWave multihop backhaul heterogeneous networks [28], maximizing the energy efficiency while guaranteeing the throughput fairness among users [29], and striking a balance between system throughput and sensor energy efficiency in UAV-assisted networks [30]. However, the aforementioned energy efficiency metric from the network-level perspective focuses on the amount of information that can be reliably transmitted per unit of energy based on the saturated traffic assumption and neglects the effects of random packet arrivals, packet queueing delay, and energy consumption during packet queueing processes.

III. System Model

In this section, we introduce mmWave UAV-assisted IAB heterogeneous cellular networks by discussing the network topology, channel model, spectrum allocation, and association strategy. The important notations in the paper are summarized in Table I.

TABLE I
Summary of Notation

Notation	Definition
$\Phi_{\mathrm{B}},\Phi_{\mathrm{I}},\Phi_{\mathrm{U}},\Phi_{\mathrm{S}},\Phi_{\mathrm{G}}$	HPPP models of the positions of MBSs, IAB nodes, UAVs, SBSs, and GUEs
$\lambda_{\mathrm{b}},\lambda_{\mathrm{i}},\lambda_{\mathrm{u}},\lambda_{\mathrm{s}},\lambda_{\mathrm{g}}$	Spatial densities of MBSs, IAB nodes, UAVs, SBSs, and GUEs
ρ	Deployment proportion of UAVs
H_{B}, H_{U}	Heights of MBSs and UAVs
a, b, β	Obstacle parameters
G_{B}, G_{U}, G_{S}, G_{G}	Main lobe antenna gains of MBSs, UAVs, and SBSs, and antenna gain of GUEs
g_{B}, g_{U}, g_{S}	Side lobe antenna gains of MBSs, UAVs, and SBSs
θ_{B}, θ_{U}, θ_{S}	Main lobe beamwidths of MBSs, UAVs, and SBSs
$F^{(\mathrm{a})},F^{(\mathrm{b})},F$	Numbers of access, backhaul, and total subchannels
η	IAB spectrum allocation coefficient
ξ	Packet arrival probability of GUEs
$P_{\mathrm{t},k}$	Transmit power of the k^{th} tier APs
α_k	Path loss exponent of access links from the k^{th} tier APs to GUEs
α_{U}, α_{S}	Path loss exponents of backhaul links from MBSs to UAVs and SBSs, respectively
m_k	Nakagami fading parameter of access links from the k^{th} tier APs to GUEs
$m_{\mathrm{U}}, m_{\mathrm{S}}$	Nakagami fading parameters of backhaul links from MBSs to UAVs and SBSs, respectively
$M_{\mathrm{B,max}}$, $M_{\mathrm{U,max}}$,$M_{\mathrm{S,max}}$	Maximum numbers of associated GUEs of MBSs, UAVs, and SBSs, respectively
$N_{\mathrm{U,max}}$, $N_{\mathrm{S,max}}$	Maximum numbers of associated UAVs and SBSs of MBSs, respectively
τ_a, τ_b	SINR and SNR thresholds of access and backhaul links, respectively

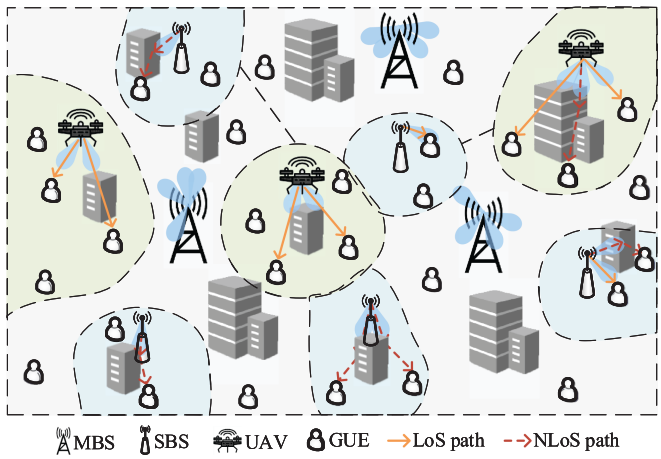

Fig. 1. Illustration of UAV-assisted heterogeneous cellular network.

A. Network Topology

As shown in Fig. 1, we consider that three types of APs (MBSs, ground SBSs, and UAVs) coexist in the UAV-assisted IAB heterogeneous cellular network. MBSs working as IAB donors connect to the core network via fiber links. The two kinds of IAB nodes (UAVs and SBSs) connect to the core network through one-hop mmWave backhaul links from MBSs. A homogeneous Poisson point process (HPPP) is used to model the spatial distribution of MBSs as Φ_{B} with density λ_{b}. The locations of IAB nodes are modeled by HPPP Φ_{I} with density λ_{i} to capture the random and irregular topology of the heterogeneous network [31], in which UAVs and SBSs are modeled by Φ_{U} and Φ_{S} with densities $\lambda_{\mathrm{u}}=\rho\lambda_{\mathrm{i}}$ and $\lambda_{\mathrm{s}}=(1-\rho)\lambda_{\mathrm{i}}$, respectively, based on the thinning property of Poisson point process (PPP) and ρ being the UAV deployment proportion. The locations of GUEs are also modeled by HPPP Φ_{G} with density λ_{g}. In this paper, as we focus on packet-level performance, we assume that GUEs are unmovable within the time by the order of magnitude of packet transmissions. Further, we consider that, the height of MBSs is H_{B}, and UAVs hover at H_{U} relative to the ground. In addition, we focus on the downlink transmissions due to the higher traffic load and larger energy overhead compared with the uplink. The uplink transmissions can be similarly studied. Our analysis is based on a typical GUE chosen from Φ_{G} at random and denoted by g, and we shift our coordinate system origin to the location of the typical GUE.

B. Channel Model

For downlink transmissions in a UAV-assisted cellular network, there exist five types of links: access link from an MBS

to a GUE (the B $\rightarrow$ G link), access link from a UAV to a GUE (the U $\rightarrow$ G link), access link from an SBS to a GUE (the S $\rightarrow$ G link), and backhaul links from an MBS to a UAV (the B $\rightarrow$ U link) and to an SBS (the B $\rightarrow$ S link). As the mmWave signal is vulnerable to occlusion, our model takes obstacles in urban areas into account. Due to the existence of obstacles, the U $\rightarrow$ G and S $\rightarrow$ G links are modeled by air-to-ground and ground-to-ground distance-dependent two-state probabilistic models, respectively. Whether the link between the typical GUE and a UAV contains an LoS path follows the probability as [32]

$$P_{\mathrm{LoS,U,G}}(r_{\mathrm{u,g}}) = \frac{1}{1 + a\exp\left[-b\left(\frac{180}{\pi}\tan^{-1}\frac{H_{\mathrm{U}}}{r_{\mathrm{u,g}}} - a\right)\right]} \quad (1)$$

where a and b are obstacle parameters related to the height, density, and area of obstacles, and $r_{\mathrm{u,g}}$ denotes the horizontal distance between the typical GUE and the UAV. The probability that the ground-to-ground link between an SBS and the typical GUE contains an LoS path follows the exponential blocking model in [33] as

$$P_{\mathrm{LoS,S,G}}(r_{\mathrm{s,g}}) = \frac{1}{\exp\left(-\frac{r_{\mathrm{s,g}}}{\beta}\right)} \quad (2)$$

where β is the obstacle parameter and $r_{\mathrm{s,g}}$ denotes the horizontal distance between the typical GUE and the SBS.

According to the thinning property of PPP and whether there is an LoS path between a UAV and the typical GUE, all UAVs can be divided into two groups relative to the typical GUE, i.e., the UAVs of LoS paths denoted by LoS UAVs and modeled as PPP $\Phi_{\mathrm{u_l}}$ with density $\lambda_{\mathrm{u_l}}(r_{\mathrm{u,g}}) = P_{\mathrm{LoS,U,G}}(r_{\mathrm{u,g}})\lambda_{\mathrm{u}}$, and the UAVs only of nonline-of-sight (NLoS) paths denoted by NLoS UAVs and modeled as PPP $\Phi_{\mathrm{u_n}}$ with density $\lambda_{\mathrm{u_n}}(r_{\mathrm{u,g}}) = [1 - P_{\mathrm{LoS,U,G}}(r_{\mathrm{u,g}})]\lambda_{\mathrm{u}}$. Similarly, all SBSs can be divided into LoS SBSs and NLoS SBSs, modeled as PPPs $\Phi_{\mathrm{S_l}}$ and $\Phi_{\mathrm{S_n}}$, with densities $\lambda_{\mathrm{s_l}}(r_{\mathrm{s,g}}) = P_{\mathrm{LoS,S,G}}(r_{\mathrm{s,g}})\lambda_{\mathrm{s}}$ and $\lambda_{\mathrm{s_n}}(r_{\mathrm{s,g}}) = [1 - P_{\mathrm{LoS,S,G}}(r_{\mathrm{s,g}})]\lambda_{\mathrm{s}}$, respectively. Thus, we model the UAV-assisted network as a heterogeneous network of five tiers of APs relative to the typical GUE. The positions of each tier's APs are modeled as PPP Φ_j with density $\lambda_j(r)$, which is equal to λ_{b}, $\lambda_{\mathrm{u_l}}(r)$, $\lambda_{\mathrm{u_n}}(r)$, $\lambda_{\mathrm{s_l}}(r)$, and $\lambda_{\mathrm{s_n}}(r)$ if $j = 1$ for MBSs, $j = 2$ for LoS UAVs, $j = 3$ for NLoS UAVs, $j = 4$ for LoS SBSs, and $j = 5$ for NLoS SBSs, respectively.

The Nakagami-m fading model is utilized to model the small-scale fading of mmWave access and backhaul links to capture the occlusion effect of obstacles [34]. Since UAVs and MBSs both have certain heights, the link between an MBS and a UAV is rather likely to contain an LoS path [35]. To simplify the analysis, the B $\rightarrow$ U link can be regarded as containing an LoS path. On the other hand, the B $\rightarrow$ G link and B $\rightarrow$ S link are considered as only NLoS paths due to the obstacles, the sparse distribution of MBSs, and the ground deployment of GUEs and SBSs [33]. Thus, the small-scale fading gains of access and backhaul links are modeled as gamma distributed random variables h with different shape and rate parameters m. Due to the nonexistence of an LoS path, the small-scale fading gains of the B $\rightarrow$ G link, the B $\rightarrow$ S link, the link from an NLoS UAV to a GUE, and the link from an NLoS SBS to a GUE can be specialized as exponential distributions.

MmWave wireless communication uses directional beams to overcome the large propagation loss [36]. Therefore, we assume that MBSs, UAVs, and SBSs are all equipped with uniform planar arrays forming directional beams and that the sectored-pattern antenna array model is adopted for analytical tractability [12]. The main lobe antenna gains of MBSs, LoS UAVs, NLoS UAVs, LoS SBSs, and NLoS SBSs are denoted as G_j within the main lobe beamwidth θ_j, and the side lobe antenna gains are g_j and $j = 1, 2, \ldots, 5$, where $G_1 = G_{\mathrm{B}}$, $G_2 = G_3 = G_{\mathrm{U}}$, $G_4 = G_5 = G_{\mathrm{S}}$, $\theta_1 = \theta_{\mathrm{B}}$, $\theta_2 = \theta_3 = \theta_{\mathrm{U}}$, $\theta_4 = \theta_5 = \theta_{\mathrm{S}}$, $g_1 = g_{\mathrm{B}}$, $g_2 = g_3 = g_{\mathrm{U}}$, and $g_4 = g_5 = g_{\mathrm{S}}$. Similar to [11], [12], we consider that GUEs are equipped with a single omnidirectional antenna with antenna gain G_{G}.

C. Spectrum Allocation

We consider that the total spectrum is partitioned into orthogonal subchannels and shared by access and backhaul links with coefficient η based on IAB. More specifically, the total bandwidth B is separated into F subchannels, and each subchannel has a bandwidth of $B_0 = B/F$. Consider that the B $\rightarrow$ G, U $\rightarrow$ G, and S $\rightarrow$ G access links share the $F^{(\mathrm{a})} = \eta F$ access subchannels. Similarly, all UAVs and SBSs share the same $F^{(\mathrm{b})} = (1 - \eta)F$ backhaul subchannels to communicate with MBSs. In each time slot, MBSs, UAVs, or SBSs randomly assign the $F^{(\mathrm{a})}$ subchannels to their associated GUEs with packets to be received. A GUE occupies at most one access subchannel for packet transmission at a time, while a UAV or an SBS can occupy all the backhaul subchannels to communicate with an MBS owing to the small interference among each other with directional beams. We further assume that within a time slot, one data packet can be transmitted on an allocated subchannel.

D. Association Strategy

The typical GUE is associated with an MBS, UAV, or SBS (denoted as the tagged MBS, UAV, or SBS) based on the maximum average received power association strategy [34]. We denote the location of the tagged AP as $\mathbf{x}^*$, which is in the k^{th} tier with $k \in \{1, 2, \ldots, 5\}$. For simplicity, $\mathbf{x}^*$ is also used as the tag of the tagged AP. The received power at the typical GUE from $\mathbf{x}^*$ can be written as

$$P_{\mathrm{r},k}(X_k) = P_{\mathrm{t},k} h_{k,\mathbf{g}} \psi_{k,\mathrm{G}} \zeta X_k^{-\alpha_k} \quad (3)$$

where $P_{\mathrm{t},k}$ is the transmit power of the k^{th} tier APs, $X_k = ||\mathbf{x}^*||$ is the distance between the tagged AP and the typical GUE, $h_{k,\mathbf{g}}$ is the small-scale fading gain from the tagged AP in the k^{th} tier to the typical GUE on the subchannel allocated to $\mathbf{g}$, $\psi_{k,\mathrm{G}} = G_k G_{\mathrm{G}}$ denotes the antenna gain of the transmission link between the tagged AP and the typical GUE, $\zeta = \left(\frac{3\times 10^8}{4\pi f_c}\right)^2$ is the path loss intercept with f_c being the carrier frequency, and α_k denotes the path loss exponent of the links from the k^{th} tier APs to the typical GUE. Considering the average received power, we have $\bar{P}_{\mathrm{r},k}(X_k) = T_k X_k^{-\alpha_k}$, where $T_k = P_{\mathrm{t},k}\bar{h}_{k,\mathbf{g}}\psi_{k,\mathrm{G}}\zeta$ with

$\bar{h}_{k,\mathbf{g}}$ denoting the average small-scale fading gain from the tagged AP to the typical GUE.

Let X_j denote the minimum distance between the typical GUE and the j^{th} tier APs. The association probability of the typical GUE associated with the tagged AP in the k^{th} tier can be derived in Appendix A as

$$A_k = 2\pi \int_0^{\infty} \lambda_k(r) r \exp\left[-2\pi \sum_{j=1}^{5} \int_0^{\widehat{r}_j} \lambda_j(r) r \mathrm{d}r\right] \mathrm{d}r \quad (4)$$

where r is the horizontal distance between the tagged AP and the typical GUE, and $\widehat{r}_j = \sqrt{\left(\frac{T_j}{T_k}\right)^{\frac{2}{\alpha_j}} \left(r^2 + H_k^2\right)^{\frac{\alpha_k}{\alpha_j}} - H_j^2}$, with H_k and H_j equal to H_{B} if $k, j = 1$, H_{U} if $k, j = 2, 3$, and 0 if $k, j = 4, 5$.

The probability density function (PDF) of the distance X_k between the typical GUE and the tagged AP in the k^{th} tier is given by Appendix B as

$$f_{X_k}(x) = \frac{2\pi}{A_k} \lambda_k \left(\sqrt{x^2 - H_k^2}\right) x \exp\left[-2\pi \sum_{j=1}^{5} \int_0^{\widehat{x}_j} \lambda_j(r) r \mathrm{d}r\right] \quad (5)$$

where $\widehat{x}_j = \sqrt{\left(\frac{T_j}{T_k}\right)^{\frac{2}{\alpha_j}} x^{\frac{2\alpha_k}{\alpha_j}} - H_j^2}$.

We consider that UAVs and SBSs are served by their nearest MBSs, named the serving MBSs. Letting $\Delta H_{\mathrm{I}}, \mathrm{I} \in \{\mathrm{U}, \mathrm{S}\}$ denote the height difference between IAB nodes and MBSs, we have $\Delta H_{\mathrm{U}} = |H_{\mathrm{U}} - H_{\mathrm{B}}|$ and $\Delta H_{\mathrm{S}} = H_{\mathrm{B}}$. The PDF of the distance Z_{I} between the tagged IAB node and its serving MBS can be derived according to (5) as

$$f_{Z_{\mathrm{I}}}(z) = 2\pi\lambda_{\mathrm{b}} z \exp\left[-\pi\lambda_{\mathrm{b}}\left(z^2 - \Delta H_{\mathrm{I}}^2\right)\right]. \quad (6)$$

Assume that the total number of GUEs associated with a k^{th} tier AP is $M_{k,0}$. Its probability mass function (PMF) is given in Appendix C as

$$\mathbb{P}(M_{k,0} = v) = \begin{cases} \frac{3.5^{3.5}\Gamma(v+3.5)\left(\frac{\lambda_{\mathrm{g}} A_1}{\lambda_{\mathrm{b}}}\right)^v}{v!\Gamma(3.5)\left(3.5+\frac{\lambda_{\mathrm{g}} A_1}{\lambda_{\mathrm{b}}}\right)^{v+3.5}}, & k = 1 \\ \frac{3.5^{3.5}\Gamma(v+3.5)\left[\frac{\lambda_{\mathrm{g}}(A_2+A_3)}{\lambda_{\mathrm{u}}}\right]^v}{v!\Gamma(3.5)\left[3.5+\frac{\lambda_{\mathrm{g}}(A_2+A_3)}{\lambda_{\mathrm{u}}}\right]^{v+3.5}}, & k = 2, 3 \\ \frac{3.5^{3.5}\Gamma(v+3.5)\left[\frac{\lambda_{\mathrm{g}}(A_4+A_5)}{\lambda_{\mathrm{s}}}\right]^v}{v!\Gamma(3.5)\left[3.5+\frac{\lambda_{\mathrm{g}}(A_4+A_5)}{\lambda_{\mathrm{s}}}\right]^{v+3.5}}, & k = 4, 5 \end{cases} \quad (7)$$

where $v \in \mathbb{N}$ denotes the number of associated GUEs, and $\Gamma(\cdot)$ is the gamma function. Due to the limited capacity of MBSs, UAVs, and SBSs, the maximum number of GUEs associated with a k^{th} tier AP is defined as $M_{k,\max}$, where $M_{1,\max} = M_{\mathrm{B},\max}$ for the MBS tier, $M_{2,\max} = M_{3,\max} = M_{\mathrm{U},\max}$ for the LoS and NLoS UAV tiers, and $M_{4,\max} = M_{5,\max} = M_{\mathrm{S},\max}$ for the LoS and NLoS SBS tiers. $M_{\mathrm{B},\max}$, $M_{\mathrm{U},\max}$, or $M_{\mathrm{S},\max}$ GUEs are selected at random if the total number of GUEs associated with an MBS, UAV, or SBS exceeds the maximum value. Thus, the PMF of the number of successfully associated GUEs of a k^{th} tier AP, M_k, is given by

$$\mathbb{P}(M_k = v) = \begin{cases} \mathbb{P}(M_{k,0} = v), v = 0, 1, \ldots, M_{k,\max} - 1 \\ \sum_{v'=v}^{\infty} \mathbb{P}(M_{k,0} = v'), \ v = M_{k,\max}. \end{cases} \quad (8)$$

The PMF of the total number of UAVs or SBSs associated with an MBS, $N_{\mathrm{I},0}, \mathrm{I} \in \{\mathrm{U},\mathrm{S}\}$, can be obtained as in (7) by

$$\mathbb{P}(N_{\mathrm{I},0} = n) = \frac{3.5^{3.5}\Gamma(n+3.5)\left(\frac{\lambda_{\mathrm{I}}}{\lambda_{\mathrm{b}}}\right)^n}{n!\Gamma(3.5)\left(3.5+\frac{\lambda_{\mathrm{I}}}{\lambda_{\mathrm{b}}}\right)^{n+3.5}}, n \in \mathbb{N}_+. \quad (9)$$

Similarly, we assume that an MBS provides backhaul support for at most $N_{\mathrm{I},\max}, \mathrm{I} \in \{\mathrm{U},\mathrm{S}\}$ UAVs/SBSs under capacity constraints. Then, the PMF of the number of successfully associated UAVs/SBSs of an MBS, $N_{\mathrm{I}}, \mathrm{I} \in \{\mathrm{U},\mathrm{S}\}$, is given by

$$\mathbb{P}(N_{\mathrm{I}} = n) = \begin{cases} \mathbb{P}(N_{\mathrm{I},0} = n), n = 0, 1, \ldots, N_{\mathrm{I},\max} - 1 \\ \sum_{n'=n}^{\infty} \mathbb{P}(N_{\mathrm{I},0} = n'), \ n = N_{\mathrm{I},\max}. \end{cases} \quad (10)$$

IV. Performance Analysis and Optimization

In this section, by leveraging stochastic geometry and queueing theory, we study the packet-level performance of mmWave UAV-assisted IAB heterogeneous cellular networks in terms of the mean packet throughput and packet energy efficiency. Then, to improve the network performance, we propose an optimization problem for maximizing the packet energy efficiency while ensuring the mean packet throughput of the network.

A. Signal Reception Quality Model

GUEs can receive signals not only from their associated APs but also from other nearby APs. Because of the spectrum sharing among the B $\rightarrow$ G, U $\rightarrow$ G, and S $\rightarrow$ G access links, the interference among access links on the same subchannel should be considered. The signal-to-interference-plus-noise ratio (SINR) at the typical GUE $\mathbf{g}$ served by the tagged AP in the k^{th} tier can be expressed as

$$\gamma_{k,\mathbf{g}}^{(\mathrm{a})} = \frac{P_{\mathrm{t},k} h_{k,\mathbf{g}} \psi_{k,\mathrm{G}} \zeta X_k^{-\alpha_k}}{\sum_{j=1}^{5} \sum_{\mathbf{x}_i \in \Phi_j \setminus \mathbf{x}^*} \delta_{j,i,\mathbf{g}} P_{\mathrm{t},j} h_{j,i,\mathbf{g}} \psi_{j,\mathrm{G}}^{(\mathrm{Int})} \zeta Y_{j,i}^{-\alpha_j} + \sigma_0 B_0} \quad (11)$$

where $\delta_{j,i,\mathbf{g}}$ is an indicator variable denoting whether the i^{th} AP in the j^{th} tier is sending packets on the same subchannel allocated to the typical GUE $\mathbf{g}$ by the tagged AP; $h_{j,i,\mathbf{g}}$ is the small-scale fading gain on the subchannel allocated to the typical GUE $\mathbf{g}$ from the i^{th} AP in the j^{th} tier to $\mathbf{g}$; $\psi_{j,\mathrm{G}}^{(\mathrm{Int})}$, equal to $G_j G_{\mathrm{G}}$ and $g_j G_{\mathrm{G}}$ with probability $\frac{\theta_j}{2\pi}$ and $1 - \frac{\theta_j}{2\pi}$, respectively, denotes the interfering antenna gain from a j^{th} tier AP to the typical GUE; $Y_{j,i}$ is the distance between the i^{th} AP in the j^{th} tier and the typical GUE; and σ_0 is the noise power spectral density.

Because of the sensitivity nature of the mmWave band to ambient noise and the high beamforming capability of MBSs, UAVs, and SBSs, similar to [12], we assume that the backhaul links are noise-limited and that the interference among backhaul links can be ignored due to the interference reduction and signal enhancement of directional antenna arrays. Then, the signal-to-noise ratio (SNR) received by the tagged IAB node from its serving MBS can be expressed as

$$\gamma_{\mathrm{I}}^{(\mathrm{b})} = \frac{P_{\mathrm{t},1} h_{\mathrm{B,I}} \psi_{\mathrm{B,I}} \zeta Z^{-\alpha_{\mathrm{I}}}}{\sigma_0 B_0}, \ \mathrm{I} \in \{\mathrm{U},\mathrm{S}\} \quad (12)$$

where $h_{\mathrm{B,I}}$, $\psi_{\mathrm{B,I}}$, and α_{I} denote the small-scale fading gain, antenna gain, and path loss exponent of the backhaul link between the tagged IAB node and its serving MBS, respectively. Given the perfect beamforming alignment between IAB nodes and MBSs, we have $\psi_{\mathrm{B,I}} = G_{\mathrm{B}}G_{\mathrm{I}}$.

B. Packet Queueing Model of Access Links

In this and the following subsections, we study the packet transmission process by analyzing the two-stage tandem queue for access and backhaul links. The discrete-time queueing model is utilized to model the packet arrivals and departures over the access and backhaul links. The early arrival model is adopted [37].

We consider that the APs maintain an access queue for one associated GUE, which can be modeled as a Geom/Geom/1 queue. Therefore, in each time slot, a packet arrives or leaves with a certain probability. To characterize the time variability of user traffic, the packet arrival process of a GUE is modeled as a Bernoulli process with tunable probability ξ, which indicates the saturation degree of traffic. Packets leave a queue according to first-in-first-out scheduling. If a packet in service fails to leave in a time slot, then it stays at the head of the queue and is retransmitted in the next available time slot.

Whether the tagged AP can successfully transmit a packet to the typical GUE depends on the subchannel contention and link quality. A GUE who has packet(s) to receive from its associated AP (or denoted as an active GUE) contends for a subchannel. The probability p_{k,M_k} that the tagged AP in the k^{th} tier with M_k successfully associated GUEs may allocate a subchannel to the typical GUE for packet transmission is given by

$$p_{k,M_k} = \min\left\{\frac{F^{(\mathrm{a})}}{\left[1-Q^{(\mathrm{a})}_{k,M_k}(0)\right](M_k-1)+1}, 1\right\} \tag{13}$$

where $Q^{(\mathrm{a})}_{k,M_k}(q)$ is the steady-state probability that the tagged AP in the k^{th} tier has q packets in the access queue for the typical GUE. According to the property of the Geom/Geom/1 queue, this can be derived as [24]

$$Q^{(\mathrm{a})}_{k,M_k}(q) = \begin{cases} 1-\xi\Big/\mu^{(\mathrm{a})}_{k,M_k}, & q=0 \\ \frac{\xi^q\left(1-\mu^{(\mathrm{a})}_{k,M_k}\right)^{q-1}\left(\mu^{(\mathrm{a})}_{k,M_k}-\xi\right)}{\left(\mu^{(\mathrm{a})}_{k,M_k}\right)^{q+1}(1-\xi)^q}, & q\in\mathbb{N}_+ \end{cases} \tag{14}$$

with $\mu^{(\mathrm{a})}_{k,M_k}$ being the packet service probability of the typical GUE by the tagged AP. Thus, $\left[1-Q^{(\mathrm{a})}_{k,M_k}(0)\right](M_k-1)$ is the average number of active GUEs served by the tagged AP except for the active typical GUE.

By considering whether the tagged AP allocates a subchannel to the typical GUE and whether the transmission of a packet on the allocated subchannel is successful, the packet service probability $\mu^{(\mathrm{a})}_{k,M_k}$ can be defined as follows:

$$\mu^{(\mathrm{a})}_{k,M_k} = p_{k,M_k}\mathbb{P}\left(\gamma^{(\mathrm{a})}_{k,\mathbf{g}} > \tau_a\right) \tag{15}$$

where $\mathbb{P}\left(\gamma^{(\mathrm{a})}_{k,\mathbf{g}} > \tau_a\right)$ is the successful transmission probability (STP) over the access link for the packet transmitted from the tagged AP to the typical GUE g, and τ_a is the SINR threshold that GUEs can successfully receive packets from APs.

Theorem 1: For the UAV-assisted IAB heterogeneous cellular network, the STP $\mathbb{P}\left(\gamma^{(\mathrm{a})}_{k,\mathbf{g}} > \tau_a\right)$ of each tier's AP over access links can be derived as

$$\mathbb{P}(\gamma^{(\mathrm{a})}_{k,\mathbf{g}} > \tau_a) = \int_{H_k}^{\infty}\sum_{c=0}^{m_k-1}\frac{s_k^c}{c!}\exp(-s_k\sigma_0 B_0)\sum_{d=0}^{c}(-1)^{2c-d}\cdot C_c^d{\sigma_0}^{c-d}{B_0}^{c-d}\frac{\mathrm{d}^d\mathcal{L}_I(s_k)}{\mathrm{d}s_k^d}f_{X_k}(x)\mathrm{d}x \tag{16}$$

where $s_k = \frac{m_k\tau_a}{P_{\mathrm{t},k}\psi_{k,G}\zeta X_k^{-\alpha_k}}$, m_k is the Nakagami fading parameter of the link between the tagged AP in the k^{th} tier and the typical GUE, $f_{X_k}(x)$ is given in (5), and $\mathcal{L}_I(s_k)$ is the Laplace transform of the total interference given by (17), as shown at the bottom of the page.

Proof: Please see Appendix D. □

In (17), $y_{\min} = \left(\frac{T_j}{T_k}\right)^{\frac{1}{\alpha_j}}X_k^{\frac{\alpha_k}{\alpha_j}}$, ${}_2F_1()$ is the Gaussian hypergeometric function, and $\mathbb{P}(\delta_{j,i,\mathbf{g}}=1)$ gives the probability that the i^{th} AP in the j^{th} tier has packet(s) to send on the same subchannel allocated to the typical GUE and is derived in Appendix E as

$$\mathbb{P}(\delta_{j,i,\mathbf{g}}=1) = \sum_{v'=1}^{M_{j,\max}}\min\left\{\frac{v'\xi}{\mu^{(\mathrm{a})}_{j,v'}F^{(\mathrm{a})}}, 1\right\}\cdot\mathbb{P}(M_j=v') \tag{18}$$

with v' being the number of GUEs associated with the i^{th} interfering AP in the j^{th} tier and $\mu^{(\mathrm{a})}_{j,v'}$ being the packet service probability of the access queues at the interfering AP. Following the same analysis approach, we can obtain $\mu^{(\mathrm{a})}_{j,v'}$ similar to $\mu^{(\mathrm{a})}_{k,M_k}$ in (15).

Remark: Theorem 1 is also suitable for an only SBS-assisted or only UAV-assisted scenario when simply setting the deployment proportion ρ equal to 0 or 1. In addition, by setting $\mathbb{P}(\delta_{j,i,\mathbf{g}}=1)=1$ in (17), the STP result can be used to evaluate the network performance under saturated traffic.

According to Little's law, the mean total time $W^{(\mathrm{a})}_{\mathrm{tot},k,M_k}$ that the tagged AP takes to successfully transmit a packet to the typical GUE equals the average number of packets in the GUE's

$$\mathcal{L}_I(s_k) = \prod_{j=1}^{5}\exp\left\{\frac{2\pi\mathbb{P}(\delta_{j,i,\mathbf{g}}=1)}{\alpha_j}\frac{\int_0^{\infty}\lambda_j(r)r\mathrm{d}r}{\int_0^{\infty}r\mathrm{d}r}\left[\begin{array}{l}\frac{\theta_j}{2\pi}\sum_{t=1}^{m_j}C^t_{m_j}(-1)^t\frac{y_{\min}^{2-\alpha_j t}(P_{\mathrm{t},j}G_jG_{\mathrm{G}}\zeta s_k)^t}{\left(t-\frac{2}{\alpha_j}\right)m_j^t}{}_2F_1\left(t,t-\frac{2}{\alpha_j};t-\frac{2}{\alpha_j}+1;-\frac{P_{\mathrm{t},j}G_jG_{\mathrm{G}}\zeta s_k}{m_j y_{\min}^{\alpha_j}}\right) \\ +\left(1-\frac{\theta_j}{2\pi}\right)\sum_{t=1}^{m_j}C^t_{m_j}(-1)^t\frac{y_{\min}^{2-\alpha_j t}(P_{\mathrm{t},j}g_jG_{\mathrm{G}}\zeta s_k)^t}{\left(t-\frac{2}{\alpha_j}\right)m_j^t}{}_2F_1\left(t,t-\frac{2}{\alpha_j};t-\frac{2}{\alpha_j}+1;-\frac{P_{\mathrm{t},j}g_jG_{\mathrm{G}}\zeta s_k}{m_j y_{\min}^{\alpha_j}}\right)\end{array}\right]\right\}. \tag{17}$$

access queue at the tagged AP $L^{(\mathrm{a})}_{\mathrm{tot},k,M_k}$ divided by the packet arrival probability, i.e., $W^{(\mathrm{a})}_{\mathrm{tot},k,M_k} = L^{(\mathrm{a})}_{\mathrm{tot},k,M_k}/\xi$.

Because $L^{(\mathrm{a})}_{\mathrm{tot},k,M_k} = \sum_{q=0}^{\infty} qQ^{(\mathrm{a})}_{k,M_k}(q)$, with some manipulation, we have

$$W^{(\mathrm{a})}_{\mathrm{tot},k,M_k} = \frac{1-\xi}{\mu^{(\mathrm{a})}_{k,M_k} - \xi}. \tag{19}$$

Remark: Equation (19) holds if the access queue is stable, i.e., $\mu^{(\mathrm{a})}_{k,M_k} > \xi$. Otherwise, $W^{(\mathrm{a})}_{\mathrm{tot},k,M_k} = \infty$.

To analyze the energy consumption during the transmission process of a packet more accurately, we take the total time $W^{(\mathrm{a})}_{\mathrm{tot},k,M_k}$ apart into packet waiting time and packet service time. The former denoted by $W^{(\mathrm{a})}_{\mathrm{wat},k,M_k}$ measures the time that a packet waits in the queue before service. The latter denoted by $W^{(\mathrm{a})}_{\mathrm{sev},k,M_k}$ includes the packet transmission delay and retransmission delay and is given by $W^{(\mathrm{a})}_{\mathrm{sev},k,M_k} = \frac{1}{\mu^{(\mathrm{a})}_{k,M_k}}$. Therefore, we have $W^{(\mathrm{a})}_{\mathrm{tot},k,M_k} = W^{(\mathrm{a})}_{\mathrm{wat},k,M_k} + W^{(\mathrm{a})}_{\mathrm{sev},k,M_k}$.

C. Packet Queueing Model of Backhaul Links

Because of the cochannel spectrum sharing among backhaul links and perfect directional transmission assumption, we consider that each backhaul link between IAB nodes and their serving MBSs occupies the same $F^{(\mathrm{b})}$ backhaul subchannels, and there is no interference or subchannel contention among the IAB nodes. Therefore, the packet service probability $\mu^{(\mathrm{b})}_{\mathrm{I}}, \mathrm{I} \in \{\mathrm{U}, \mathrm{S}\}$ on a subchannel of the backhaul link from the serving MBS to the tagged IAB node equals the STP over the backhaul link, which, according to Appendix F, can be derived as

$$\mu^{(\mathrm{b})}_{\mathrm{I}} = \int_{\Delta H_{\mathrm{I}}}^{\infty} 2\pi\lambda_{\mathrm{b}} z \sum_{c=0}^{m_{\mathrm{I}}-1} \frac{\left(\frac{m_{\mathrm{I}}\tau_b\sigma_0 B_0}{P_{\mathrm{t},1}\psi_{\mathrm{B,I}}\zeta z^{-\alpha_{\mathrm{I}}}}\right)^c}{c!} \cdot \exp\left[-\frac{m_{\mathrm{I}}\tau_b\sigma_0 B_0}{P_{t,1}\psi_{\mathrm{B,I}}\zeta z^{-\alpha_{\mathrm{I}}}} - \pi\lambda_{\mathrm{b}}(z^2 - \Delta H_{\mathrm{I}}^2)\right] \mathrm{d}z \tag{20}$$

with m_{I} being the Nakagami fading parameter of the backhaul link between the tagged IAB node and its serving MBS and τ_b being the SNR threshold for IAB nodes to successfully receive packets from MBSs.

For the backhaul queue, we consider that all packets arriving at the serving MBS and belonging to the GUEs associated with the same UAV or SBS are stored in a single large queue. Generally, the probability that two or more packets for different GUEs arrive simultaneously at the queue is small [38]. Thus, we assume that in each slot, at most one packet arrives at the backhaul queue for the tagged IAB node at the serving MBS, and the total packet arrival probability is then ξM_k conditioned on M_k GUEs associated with the tagged IAB node. Then, the backhaul queue from the serving MBS to the tagged IAB node can be characterized as a Geom/Geom/s queue with packet arrival probability ξM_k and $s = F^{(\mathrm{b})}$ servers. Here, each server has packet service probability $\mu^{(\mathrm{b})}_{\mathrm{I}}$.

The steady-state probability $Q^{(\mathrm{b})}_{k,M_k}(d)$ that there are d packets in the backhaul queue for the tagged IAB node serving the typical GUE can be derived by Markov-based analysis and solving difference equations according to the property of the Geom/Geom/s queue [37] provided that the queue is stable, i.e., $F^{(\mathrm{b})}\mu^{(\mathrm{b})}_{\mathrm{I}} > \xi M_k$.

According to Little's law, the average total time $W^{(\mathrm{b})}_{\mathrm{tot},k,M_k}$ that a packet spends in the backhaul queue equals the average total number of packets in the queue $L^{(\mathrm{b})}_{\mathrm{tot},k,M_k}$ divided by the total packet arrival probability, i.e.,

$$W^{(\mathrm{b})}_{\mathrm{tot},k,M_k} = \frac{L^{(\mathrm{b})}_{\mathrm{tot},k,M_k}}{\xi M_k} \tag{21}$$

where $L^{(\mathrm{b})}_{\mathrm{tot},k,M_k} = \sum_{d=0}^{\infty} dQ^{(\mathrm{b})}_{k,M_k}(d)$.

Remark: Equation (21) holds if the backhaul queue is stable; otherwise, $W^{(\mathrm{b})}_{\mathrm{tot},k,M_k} = \infty$. Different from $W^{(\mathrm{a})}_{\mathrm{tot},k,M_k}$ in (19), $W^{(\mathrm{b})}_{\mathrm{tot},k,M_k}$ should be numerically calculated, as the steady-state probability $Q^{(\mathrm{b})}_{k,M_k}(d)$ has no closed-form solution.

The packet service time $W^{(\mathrm{b})}_{\mathrm{sev},k,M_k}$ of the backhaul queue from the serving MBS to the tagged IAB node is given by $W^{(\mathrm{b})}_{\mathrm{sev},k,M_k} = \frac{1}{\mu^{(\mathrm{b})}_{\mathrm{I}}}$, where $\mu^{(\mathrm{b})}_{\mathrm{I}} = \mu^{(\mathrm{b})}_{\mathrm{U}}$ if $k = 2, 3$, and $\mu^{(\mathrm{b})}_{\mathrm{I}} = \mu^{(\mathrm{b})}_{\mathrm{S}}$ if $k = 4, 5$.

D. MPT and PEE Analysis

In this subsection, we study the MPT and PEE of GUEs. The MPT $\mathcal{T}$ is defined as the reciprocal of the average time to successfully deliver a packet from an MBS to a GUE, and the PEE $\mathcal{E}$ is defined as the reciprocal of the mean total energy consumed by a packet for successful delivery, both via one-hop or two-hop transmissions in the network of interest.

Theorem 2: For a UAV-assisted IAB heterogeneous cellular network with the two-stage tandem queues, the MPT $\mathcal{T}_{k,M_k}$ of the typical GUE associated with the tagged AP in the k^{th} tier and of M_k associated GUEs is given by

$$\mathcal{T}_{k,M_k} = \begin{cases} \frac{1}{W^{(\mathrm{a})}_{\mathrm{tot},k,M_k}}, & \text{if; } \mu^{(\mathrm{a})}_{k,M_k} > \xi, k = 1 \\ \frac{1}{W^{(\mathrm{a})}_{\mathrm{tot},k,M_k} + W^{(\mathrm{b})}_{\mathrm{tot},k,M_k}}, & \text{if } F^{(\mathrm{b})}\mu^{(\mathrm{b})}_{\mathrm{I}} > \xi M_k \text{; and} \\ & \mu^{(\mathrm{a})}_{k,M_k} > \xi, k = 2, 3, 4, 5 \\ 0, & \text{if } F^{(\mathrm{b})}\mu^{(\mathrm{b})}_{\mathrm{I}} \le \xi M_k \text{ or } \mu^{(\mathrm{a})}_{k,M_k} \le \xi, k = 1, 2, \ldots, 5. \end{cases} \tag{22}$$

Proof: This can be proven by considering three cases: 1) the GUE is associated with the MBS, and thus only the delay in the access queue is counted; 2) the GUE is associated with an IAB node, and both the access queue and backhaul queue are stable; and 3) the GUE is associated with an AP with either or both unstable access and backhaul queues. □

Then, by averaging over the tagged AP's tier options and the number of its associated GUEs, the MPT of the typical GUE can

be given by

$$\mathcal{T} = \sum_{k=1}^{5} A_k \sum_{v=1}^{M_{k,\max}} \frac{\mathbb{P}(M_k = v)}{1 - \mathbb{P}(M_k = 0)} \mathcal{T}_{k,v}. \tag{23}$$

Remark: The MPT characterizes network performance from the perspective of the whole packet transmission process, including the random packet arrivals, dynamic queueing processes, packet service processes, transmission failures, and packet retransmissions. In the UAV-assisted IAB heterogeneous cellular network, its value is affected by traffic load and queueing and transmission delay in both access and backhaul queues.

In the transmission process, a packet of the typical GUE consumes both the basic operation energy and the transmit energy of the tagged AP and the serving MBS, if any, for packet queueing, transmission, and reception. Moreover, an AP may serve multiple packets simultaneously. Thus, from the packet-level point of view, its basic operation energy is consumed by all arrival packets.

Proposition 1: If the typical GUE is associated with an MBS, then the mean energy consumption per packet from the moment that the packet arrives at the tagged MBS to its successful delivery to the typical GUE can be written as

$$\bar{E}_1 = P_{\mathrm{t},1} t_{\mathrm{slot}} \bar{W}^{(\mathrm{a})}_{\mathrm{sev},1} + \frac{P_{\mathrm{bsc,B}} t_{\mathrm{slot}}}{\bar{L}_{\mathrm{B}}} \bar{W}^{(\mathrm{a})}_{\mathrm{tot},1}. \tag{24}$$

Here, t_{slot} is the length of one time slot for packet transmission; $P_{\mathrm{bsc,B}}$ is the basic operation power of MBSs including the signal process, power amplifier, cooling, etc.; $\bar{L}_{\mathrm{B}}$, given in (25) and shown at the bottom of this page, is the average total number of packets in the access and backhaul queues at the MBS; and $\bar{W}^{(\mathrm{a})}_{\mathrm{sev},1}$ and $\bar{W}^{(\mathrm{a})}_{\mathrm{tot},1}$ are the mean service time and the total time a packet of the typical GUE spending in its access queue at the tagged MBS, respectively. This can be calculated as follows by averaging over the number of associated GUEs and setting k to 1:

$$\bar{W}^{(\mathrm{a})}_{\mathrm{sev},k} = \sum_{v=1}^{M_{k,\max}} \frac{\mathbb{P}(M_k = v)}{1 - \mathbb{P}(M_k = 0)} W^{(\mathrm{a})}_{\mathrm{sev},k,v} \tag{26a}$$

$$\bar{W}^{(\mathrm{a})}_{\mathrm{tot},k} = \sum_{v=1}^{M_{k,\max}} \frac{\mathbb{P}(M_k = v)}{1 - \mathbb{P}(M_k = 0)} W^{(\mathrm{a})}_{\mathrm{tot},k,v}. \tag{26b}$$

Proof: The proposition can be proven by accumulating the energy consumption of packet transmissions in two stages: one from the packet arrival to the end of waiting in the queue and the other during the packet transmission. Note that when evaluating the energy consumption in the first stage, one needs to count the total number of packets buffered in the MBS, not only for the associated GUEs but also for the associated UAVs and SBSs, as shown in (25). □

Proposition 2: If the typical GUE is associated with a UAV (i.e., $k=2,3$), then the mean energy consumption per packet from the moment that the packet arrives at the serving MBS to its successful delivery to the typical GUE via the tagged UAV can be expressed as

$$\bar{E}_k = P_{\mathrm{t},1} t_{\mathrm{slot}} \bar{W}^{(\mathrm{b})}_{\mathrm{sev},k} + \frac{P_{\mathrm{bsc,B}} t_{\mathrm{slot}}}{\bar{L}_{\mathrm{B}}} \bar{W}^{(\mathrm{b})}_{\mathrm{tot},k} + P_{\mathrm{t},k} t_{\mathrm{slot}} \cdot \bar{W}^{(\mathrm{a})}_{\mathrm{sev},k} + \frac{(P_{\mathrm{bsc,U}} + P_{\mathrm{hov}}) t_{\mathrm{slot}}}{\bar{L}_{\mathrm{U}}} \bar{W}^{(\mathrm{a})}_{\mathrm{tot},k}, k = 2, 3 \tag{27}$$

where $P_{\mathrm{bsc,U}}$ is the basic operation power of UAVs, P_{hov} is the UAV hovering power, and $\bar{W}^{(\mathrm{b})}_{\mathrm{sev},k}$ and $\bar{W}^{(\mathrm{b})}_{\mathrm{tot},k}$ are the mean service time and the total time a packet of the typical GUE spending in the backhaul queue, respectively. These are given as follows:

$$\bar{W}^{(\mathrm{b})}_{\mathrm{sev},k} = \sum_{v=1}^{M_{k,\max}} \frac{\mathbb{P}(M_k = v)}{1 - \mathbb{P}(M_k = 0)} W^{(\mathrm{b})}_{\mathrm{sev},k,v} \tag{28a}$$

$$\bar{W}^{(\mathrm{b})}_{\mathrm{tot},k} = \sum_{v=1}^{M_{k,\max}} \frac{\mathbb{P}(M_k = v)}{1 - \mathbb{P}(M_k = 0)} W^{(\mathrm{b})}_{\mathrm{tot},k,v}, \tag{28b}$$

and $\bar{L}_{\mathrm{U}}$ is the average total number of packets in the access queues at the tagged UAV, satisfying

$$\bar{L}_{\mathrm{U}} = \sum_{v_{\mathrm{u,g}}=0}^{M_{k,\max}} v_{\mathrm{u,g}} \sum_{j=2}^{3} \frac{A_j}{A_2 + A_3} L^{(\mathrm{a})}_{\mathrm{tot},j,v_{\mathrm{u,g}}} \mathbb{P}(M_k = v_{\mathrm{u,g}}). \tag{29}$$

Proof: If the typical GUE is associated with an IAB node, then the transmission of a packet consumes not only the basic and transmit power of the serving MBS for backhaul but also the basic and transmit power of the tagged IAB node for access. If the tagged IAB node is a UAV, in addition to the basic operation power $P_{\mathrm{bsc,U}}$, extra hovering power P_{hov} is needed.

Furthermore, when counting the total number of packets consuming the UAV's energy, as shown in (29), the following factors are considered, i.e., the number of associated GUEs, number of packets in each GUE's access queue, and whether the UAV is an LoS or NLoS UAV with respect to the associated GUEs. □

Corollary 1: If the typical GUE is associated with an SBS (i.e., $k = 4, 5$), the mean energy consumption per packet from the moment that the packet arrives at the serving MBS to its successful delivery to the typical GUE via the tagged SBS can

$$\bar{L}_{\mathrm{B}} = \sum_{v_{\mathrm{b,g}}=0}^{M_{\mathrm{B},\max}} v_{\mathrm{b,g}} L^{(\mathrm{a})}_{\mathrm{tot},1,v_{\mathrm{b,g}}} \mathbb{P}(M_1 = v_{\mathrm{b,g}}) + \sum_{n_{\mathrm{b,u}}=0}^{N_{\mathrm{U},\max}} \sum_{v_{\mathrm{u,g}}=0}^{M_{\mathrm{U},\max}} L^{(\mathrm{b})}_{\mathrm{tot},2,v_{\mathrm{u,g}}} \mathbb{P}(M_2 = v_{\mathrm{u,g}}) n_{\mathrm{b,u}} \mathbb{P}(N_{\mathrm{U}} = n_{\mathrm{b,u}}) + \sum_{n_{\mathrm{b,s}}=0}^{N_{\mathrm{S},\max}} \sum_{v_{\mathrm{s,g}}=0}^{M_{\mathrm{S},\max}} L^{(\mathrm{b})}_{\mathrm{tot},4,v_{\mathrm{s,g}}} \mathbb{P}(M_4 = v_{\mathrm{s,g}}) n_{\mathrm{b,s}} \mathbb{P}(N_{\mathrm{S}} = n_{\mathrm{b,s}}). \tag{25}$$

be written as

$$\bar{E}_k = P_{\mathrm{t},1} t_{\mathrm{slot}} \bar{W}^{(\mathrm{b})}_{\mathrm{sev},k} + \frac{P_{\mathrm{bsc,B}} t_{\mathrm{slot}}}{\bar{L}_{\mathrm{B}}} \bar{W}^{(\mathrm{b})}_{\mathrm{tot},k} + P_{\mathrm{t},k} t_{\mathrm{slot}} \cdot \bar{W}^{(\mathrm{a})}_{\mathrm{sev},k} + \frac{P_{\mathrm{bsc,S}} t_{\mathrm{slot}}}{\bar{L}_{\mathrm{S}}} \bar{W}^{(\mathrm{a})}_{\mathrm{tot},k}, k = 4, 5 \quad (30)$$

where $\bar{L}_{\mathrm{S}}$ is the average total number of packets in the access queues at the SBS, satisfying

$$\bar{L}_{\mathrm{S}} = \sum_{v_{\mathrm{s,g}}=0}^{M_{k,\max}} v_{\mathrm{s,g}} \sum_{j=4}^{5} \frac{A_j}{A_4 + A_5} L^{(\mathrm{a})}_{\mathrm{tot},j,v_{\mathrm{s,g}}} \mathbb{P}(M_k = v_{\mathrm{s,g}}). \quad (31)$$

We omit the proof as it is similar to the one for Proposition 2. Based on Propositions 1 and 2 and Corollary 1, the following theorem is straightforward.

Theorem 3: For the UAV-assisted heterogeneous cellular network with two-stage tandem queues, the PEE of the typical GUE is obtained by averaging over the tagged AP's tier option as

$$\mathcal{E} = \sum_{k=1}^{5} A_k \frac{1}{\bar{E}_k}. \quad (32)$$

Remark: The PEE captures the total energy consumption (including both communication-related and communication-unrelated energy) of a packet from its generation at an MBS to the successful delivery to a GUE through one- or two-hop transmissions, if any. In the UAV-assisted IAB heterogeneous cellular network, its value is affected by not only the packet queueing and service delay but also packet accumulation at APs. Compared with the conventional network-level energy efficiency metric that is defined as the mean number of successfully transmitted packets divided by the total energy consumption, the PEE also captures the energy consumption of the packets waiting in the two-stage tandem queues in addition to that of the packets being transmitted.

E. Performance Optimization

In the mmWave UAV-assisted IAB heterogeneous cellular network, the UAV height H_{U}, IAB node density λ_{i}, UAV deployment proportion ρ, and IAB spectrum allocation coefficient η are key network configuration parameters. H_{U} impacts both the probability of establishing an LoS link and the path loss. λ_{i} determines the density of IAB nodes that assist the macrocell networks, including UAVs and ground SBSs. ρ affects the proportion of UAVs to all IAB nodes. η is used to adjust the subchannel allocation between access and backhaul links. To optimize the UAV deployment and network configuration, we establish the following single-objective optimization problem, aiming at maximizing the packet-level energy efficiency performance under the throughput requirement

$$\max_{H_{\mathrm{U}},\lambda_{\mathrm{i}},\rho,\eta} \quad \mathcal{E} \quad \text{s.t.} \quad \mathcal{T} > \mathcal{T}_{\mathrm{th}} \quad (33)$$

where $\mathcal{T}_{\mathrm{th}}$ is the required MPT threshold. Because of the complicated analytical expressions under random spatiotemporal traffic, the problem in (33) can hardly be directly solved. Therefore, we resort to the alternating optimization approach to find a good network configuration by iteratively optimizing the PEE with respect to the key network parameters. Specifically, for the ease of intuitive illustration by figures, we divide the key network parameters into two variable blocks $(H_{\mathrm{U}}, \lambda_{\mathrm{i}})$ and (ρ, η) in the alternating optimization, which is the same as iterating over the four variables individually as long as the decoupling among variable blocks is ensured [39]. In each iteration, on the premise of satisfying the MPT requirement, we update $(H_{\mathrm{U}}, \lambda_{\mathrm{i}})$ by maximizing PEE with (ρ, η) fixed to the values obtained in the last iteration. Then, we obtain (ρ, η) by maximizing PEE with $(H_{\mathrm{U}}, \lambda_{\mathrm{i}})$ fixed to the updated values in the current iteration. The procedure is repeated to adjust the parameters until the PEE converges. In addition, the finite range and appropriate granularity for the parameters are adopted to implement the iterative procedure within an acceptable amount of computation.

TABLE II
SYSTEM PARAMETERS

Parameter	Value	Parameter	Value
λ_{b}, λ_{i}, λ_{g}	$2\times10^{-5}/\mathrm{m}^2$, $1\times10^{-4}/\mathrm{m}^2$, $5\times10^{-3}/\mathrm{m}^2$	$P_{\mathrm{t},1}$, $P_{\mathrm{t},2}$, $P_{\mathrm{t},3}$, $P_{\mathrm{t},4}$, $P_{\mathrm{t},5}$	10 W, 1 W, 1 W, 1 W, 1 W
H_{B}, H_{U}	10 m, 70 m	a, b, β	11.95,0.136,20
$P_{\mathrm{bsc,B}}$,$P_{\mathrm{bsc,U}}$, $P_{\mathrm{bsc,S}}$,P_{hov}	4000 W,2000 W, 2000 W,1000 W	G_{B}, G_{U}, G_{S}, G_{G}	18 dB, 18 dB, 18 dB, 0 dB
θ_{B}, θ_{U}, θ_{S}	20°, 20°, 20°	g_{B}, g_{U}, g_{S}	−2 dB,−2 dB, −2 dB
α_1,α_2,α_3, α_4,α_5,α_{U},α_{S}	4, 3, 4, 3, 4, 3, 4	m_1,m_2,m_3, m_4,m_5,m_{U},m_{S}	1, 3, 1, 3, 1, 3, 1
$M_{\mathrm{B,max}}$, $M_{\mathrm{U,max}}$, $M_{\mathrm{S,max}}$	50, 10, 10	$N_{\mathrm{U,max}}$, $N_{\mathrm{S,max}}$	10, 10
f_c, B	28 GHz,3 GHz	F	10
ξ	0.1	σ_0	−174 dBm/Hz
ρ	0.5	η	0.5
τ_a, τ_b	0 dB,10 dB	t_{slot}	1ms

V. NUMERICAL RESULTS AND DISCUSSIONS

In this section, we provide numerical results to investigate the MPT and PEE performance of the mmWave UAV-assisted IAB heterogeneous cellular network. The theoretical analysis is validated via 3000 Monte Carlo simulations. The simulation area is 1000×1000 m^2, and each realization includes 5000 continuous time slots. Unless otherwise stated, the parameter values used in simulations are listed in Table II [12], [24], [33], [34].

Fig. 2 shows how the GUEs associate with the five tiers of APs as the UAV height changes, given the UAV deployment proportion ρ equal to 0.5. As seen in the figure, when UAVs are at the same altitude as MBSs (i.e., 10 m), MBSs play a crucial part in serving GUEs because at a low height, most of the LoS paths between UAVs and GUEs are blocked by obstacles, leading to no large advantage for UAVs over ground MBSs in providing high-quality signals with lower transmit power. At a higher height (e.g., $H_{\mathrm{U}} \leq 70$ m), the UAVs' association probability increases significantly, as they can avoid obstacles and establish LoS paths with GUEs, which greatly improves the received signal quality. However, as the height of UAVs continues to rise, the distance

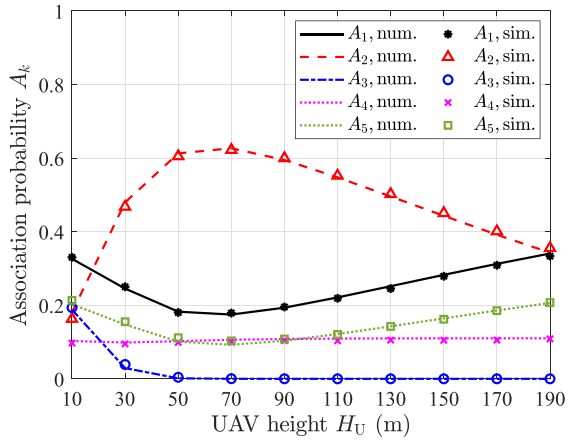

Fig. 2. Association probability of 5 tiers of APs vs. UAV height.

between UAVs and GUEs increases, and the LoS paths in the U $\rightarrow$ G links suffer greatly from the long-distance propagation loss over the mmWave band. Hence, the association probability of UAVs decreases and that of MBSs and SBSs increases.

It is also noteworthy that a portion of SBSs can provide LoS links and are closer to GUEs than UAVs due to the ground deployment, implying that the UAV's advantage of high altitude decreases. Thus, the association probability of LoS SBSs is independent of the increase in UAV height. In addition, with high height, low transmit power, and severe attenuation, NLoS UAVs have no opportunity to provide reliable access service when UAVs hover at a relatively high altitude.

In Fig. 3, we validate the numerical results of the MPT and PEE with Monte Carlo simulations and study the impact of UAV height under different deployment proportions of UAVs. The simulation results agree well with the numerical results. Compared with the only SBS-assisted network, the heterogeneous network of three kinds of APs can significantly improve the MPT performance with the assistance of aerial UAVs. Adjusting their height, UAVs can avoid the obstruction of buildings and establish high-quality LoS access and backhaul links with GUEs and MBSs, respectively, while the low-altitude SBSs cannot. Moreover, from Fig. 3(a), we notice that the MPT of GUEs increases and then decreases with an increase in UAV height. The reason is similar to that of the changing trend of the association probability of LoS UAVs. Although UAVs have the advantage of flexibly accommodating spatiotemporal network traffic, they consume extra communication-unrelated energy to hover in the air; thus, a larger deployment proportion ρ of UAVs causes lower energy efficiency. Because of this, in Fig. 3(b), the PEE reaches the nadir at the UAV height where association with UAVs is preferred, as shown in Fig. 2. In general, the UAV-assisted heterogeneous cellular network offers a new way by adjusting the proportion of UAVs replacing SBSs and the UAV height to achieve a better trade-off between throughput and energy efficiency performance.

In Figs. 4 and 5, we study the impact of UAV deployment proportion ρ on the MPT and PEE performance under different traffic loads, measured in GUE density and packet arrival probability, respectively. Since the accuracy of our analytical

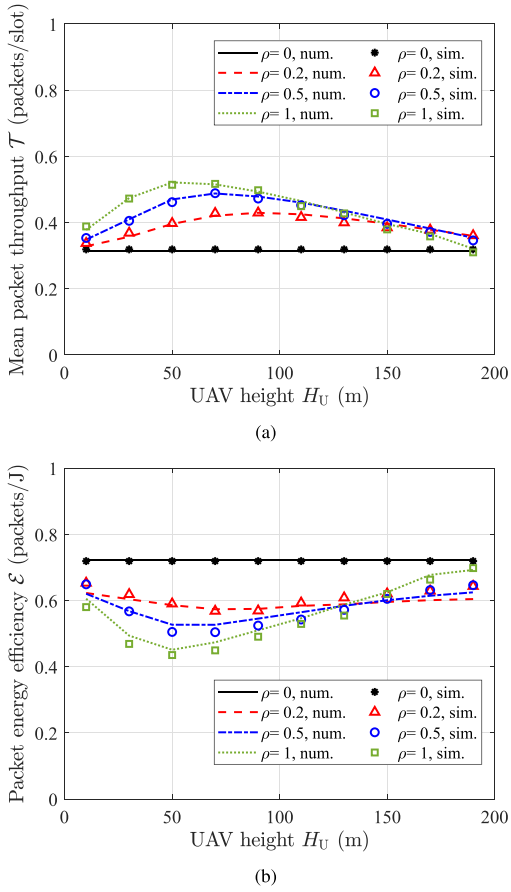

Fig. 3. Network performance under different UAV heights and UAV deployment proportions: (a) MPT; (b) PEE.

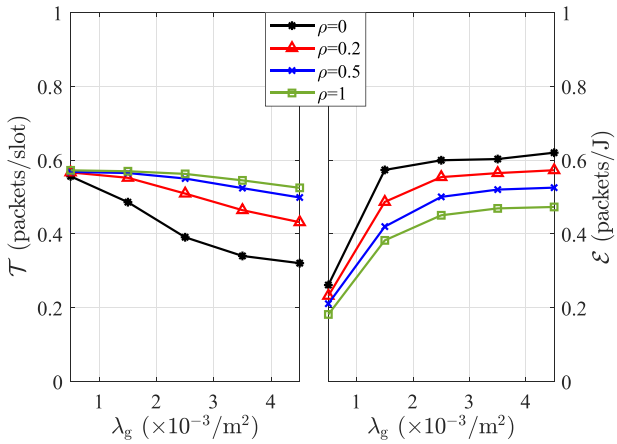

Fig. 4. MPT and PEE vs. GUE density under different UAV deployment proportions.

model has been verified and the analysis matches well with the simulation results, unless otherwise stated, in the following we provide numerical results to investigate the two performance metrics. As shown from the figures, with an increase in the traffic load, the MPT decreases while the PEE increases. The greater the number of GUEs or the larger the packet arrival probability, the more severe the spectrum contention and the more aggravated the interference, leading to a reduced MPT. In

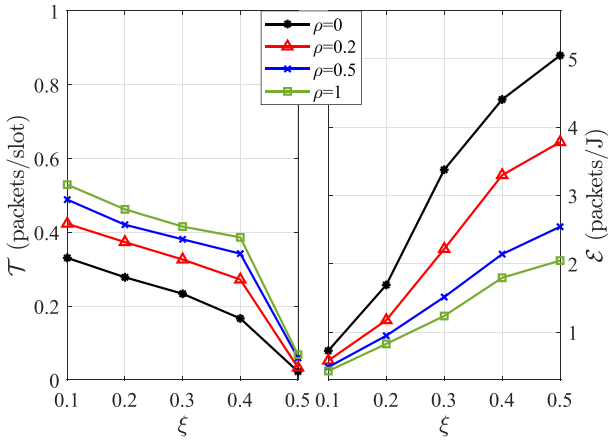

Fig. 5. MPT and PEE vs. packet arrival probability under different UAV deployment proportions.

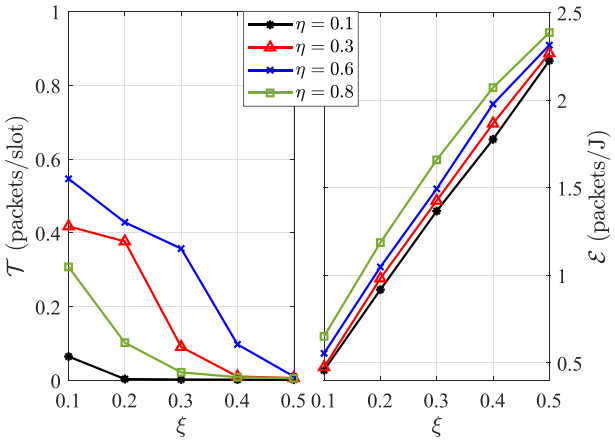

Fig. 6. MPT and PEE vs. packet arrival probability under different IAB spectrum allocation coefficients.

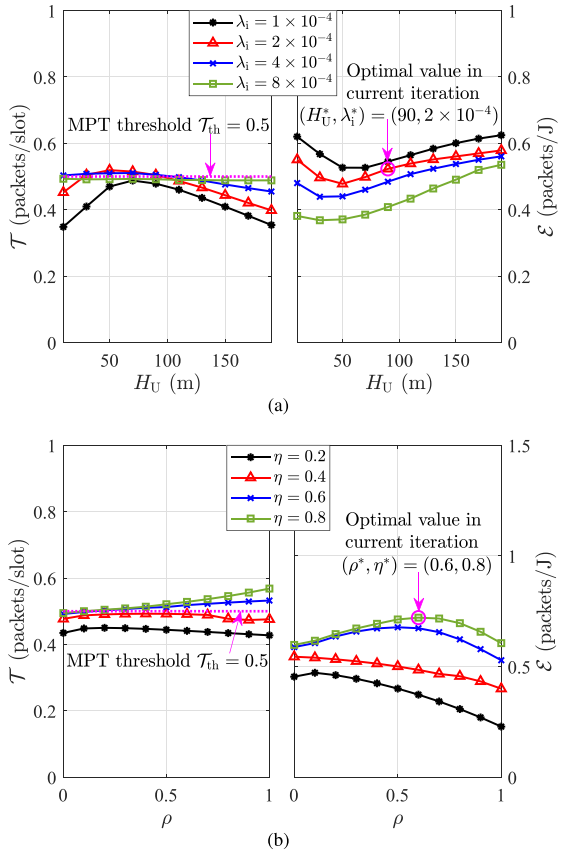

Fig. 7. Performance optimization in first iteration: (a) MPT and PEE vs. UAV height under different IAB node densities; (b) MPT and PEE vs. UAV deployment proportion under different IAB spectrum allocation coefficients.

contrast, if the traffic load is low, in each slot, a small number of packets served by APs need to share the total energy cost, including both communication-related and communication-unrelated energy, generating a low PEE. Note that increasing the UAV deployment proportion can improve MPT but reduce PEE due to the improved link quality and increased UAV hovering energy, respectively. In addition, as illustrated in Fig. 4, the MPT tends to converge as the GUE density increases due to the constraints of the APs' capacity. On the other hand, as shown in Fig. 5, as the packet arrival probability increases, the MPT approaches zero due to the heavy traffic load, the massive packet accumulation in the queues, and the sharply increased queueing delay. One may also notice from the two figures that the performance improvement of MPT decreases as the UAV deployment proportion increases, implying the importance of an appropriate choice of the UAV deployment proportion.

Fig. 6 shows how the MPT and PEE performance is affected by the spectrum allocation between access and backhaul links under different packet arrival probabilities ξ. It can be observed from the figure that with sufficient subchannels for backhaul, more subchannels for the access links (i.e., a relatively large spectrum allocation coefficient η) render a higher MPT. This is rational because, owing to the omnidirectional antennas of GUEs, the access links suffer from worse interference than the backhaul links, resulting in the larger requirement for subchannels. However, too few subchannels for backhaul (i.e., $\eta = 0.8$) lead to poor MPT because of the transmission bottleneck caused by the backhaul links. On the other hand, it is noteworthy from Fig. 6 that, with more subchannels for access links, the queueing delay of packets in the access queues at the APs is reduced, leading to a reduced energy consumption at UAVs or SBSs and an improved PEE. From Fig. 6, we find that the MPT and PEE performance can be simultaneously improved by appropriately setting the spectrum allocation scheme of the IAB technology.

To understand how the packet-level energy efficiency of the mmWave UAV-assisted IAB heterogeneous cellular network can be improved while offering packet throughput assurance, Figs. 7 and 8 show the searching process of the first iteration for optimization problem (33) and how the PEE changes with the iteration number based on the alternating optimization approach, respectively. Here, we set the key network parameters with finite values within reasonable ranges as $H_U \in \{10, 30, \ldots, 190\}$m, $\lambda_i \in \{1, 2, \ldots, 10\} \times 10^{-4}/\text{m}^2$, $\rho \in \{0, 0.1, \ldots, 1\}$, and $\eta \in \{0.1, 0.2, \ldots, 0.9\}$, and we omit some values of the parameters in Fig. 7 for readability. Specifically, in Fig. 7(a), we present how the MPT and PEE change with the adjustment of the IAB

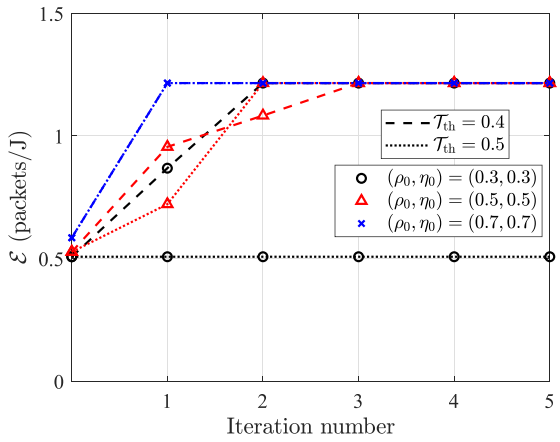

Fig. 8. PEE vs. iteration number under different MPT thresholds and initial values of ρ and η.

node density $\lambda_{\rm i}$ and the UAV height $H_{\rm U}$, given the MPT threshold $\mathcal{T}_{\rm th} = 0.5$ and the initial values of the UAV deployment proportion and IAB spectrum allocation coefficient $(\rho_0, \eta_0) = (0.5, 0.5)$. By maximizing the PEE performance under the required MPT, the optimal UAV height and IAB node density in the current iteration can be obtained as $(H_{\rm U}^*, \lambda_{\rm i}^*) = (90, 2 \times 10^{-4})$. As illustrated in the figure, with the increase in the density of IAB nodes, the MPT improves before reaching a critical value. However, continuing to increase the density does not improve the MPT performance; instead, the MPT degrades due to the increase in interference. On the other hand, in addition to dramatically increasing the deployment and maintenance costs, overintensive deployment of IAB nodes results in lower PEE, as shown in Fig. 7(a). This is because the denser deployment of IAB nodes attracts more GUEs connecting to them, rather than the one-hop MBSs. However, the two-hop communication undoubtedly consume more energy from not only MBSs but also IAB nodes for packet transmission and processing, thus decreasing the energy efficiency. We can find from the figure that an appropriate choice of IAB node density and UAV height can enhance both the packet throughput and energy efficiency performance.

Given the optimal value of UAV height and IAB node density $(H_{\rm U}^*, \lambda_{\rm i}^*)$ obtained in Fig. 7(a) in the current iteration, Fig. 7(b) then depicts how to appropriately set the UAV deployment proportion ρ and IAB spectrum allocation coefficient η to improve the MPT and PEE performance. By optimizing ρ and η under the required MPT, one can iteratively obtain better PEE performance compared with Fig. 7(a) with (ρ^*, η^*) equal to (0.6, 0.8). As shown in the figure, in the current setting, increasing the UAV deployment proportion has no significant effect on MPT enhancement; in contrast, a high UAV proportion can deteriorate the PEE due to the extra communication-unrelated energy consumption. The reason for this is that with a dense IAB node deployment $\lambda_{\rm i}^*$, SBSs get closer to GUEs and are capable of providing the same LoS coverage that UAVs can offer in the air, thus reducing the dependence on UAVs. Furthermore, the dense deployment reduces the backhaul load of IAB nodes while aggravating the interference over access links. Thus, a larger IAB spectrum allocation coefficient (e.g., $\eta = 0.8$) contributes to the improvement of both MPT and PEE performance. To study the optimal network configuration under the parameter values we focused on, Fig. 8 then illustrates that the PEE increases with the iteration number based on three initial values of ρ and η and two MPT thresholds $\mathcal{T}_{\rm th}$. The PEE converges very fast under different initial values and MPT thresholds, and the performance improvement of PEE can be up to 140%. Moreover, appropriate initial values can accelerate the optimization process and enhance the PEE performance. Note that the undue requirement for MPT performance may cause suboptimal PEE under small initial values, i.e., $(\rho_0, \eta_0) = (0.3, 0.3)$ and $\mathcal{T}_{\rm th} = 0.5$ owing to the difficulty of further finding improved PEE with stringent MPT requirements.

VI. Conclusion

In this paper, we have proposed an analytical framework for investigating mmWave UAV-assisted IAB heterogeneous cellular networks' performance in terms of packet-level throughput and energy efficiency based on stochastic geometry and queueing theory. The studied packet-level performance metrics capture both the spatial randomness of node deployments and the temporal randomness of user traffic. The numerical results have demonstrated that the mmWave UAV-assisted IAB heterogeneous cellular network can strike a good balance between throughput and energy efficiency performance or even achieve a win-win result. For future work, the analytical framework can be extended to study the packet-level performance of the network with other GUE/UAV distributions and/or moving UAVs.

Appendix A
Proof of (4)

The probability that the associated AP of the typical GUE is in the $k^{\rm th}$ tier is given as

$$\begin{aligned} A_k &= \mathbb{E}_{X_k}\left[\bar{P}_{r,k}(X_k) > \max_{j, j\neq k} \bar{P}_{r,j}(X_j)\right] \\ &= \mathbb{E}_{R_k}\left\{\prod_{j=1, j\neq k}^{5} \mathbb{P}\left[\sqrt{R_j^2 + H_j^2} > \left(\frac{T_j}{T_k}\right)^{\frac{1}{\alpha_j}} \times \sqrt{{R_k}^2 + H_k^2}^{\frac{\alpha_k}{\alpha_j}}\right]\right\} \\ &= \int_0^\infty \prod_{\substack{j=1, \\ j\neq k}}^{5} \mathbb{P}\left[R_j > \sqrt{\left(\frac{T_j}{T_k}\right)^{\frac{2}{\alpha_j}} (r^2 + H_k^2)^{\frac{\alpha_k}{\alpha_j}} - H_j^2}\right] \times f_{R_k}(r)\mathrm{d}r \\ &\overset{(a)}{=} 2\pi \int_0^\infty \lambda_k(r) r \exp\left[-2\pi \sum_{j=1}^{5} \int_0^{\widehat{r}_j} \lambda_j(r) r \mathrm{d}r\right] \mathrm{d}r \end{aligned} \quad (34)$$

where R_j denotes the minimum horizontal distance between the $j^{\rm th}$ tier APs and the typical GUE, $\widehat{r}_j =$

$\sqrt{\left(\frac{T_j}{T_k}\right)^{\frac{2}{\alpha_j}}(r^2+H_k^2)^{\frac{\alpha_k}{\alpha_j}}-H_j^2}$, and equation (a) holds because according to the distance property of PPP, the complementary cumulative distribution function (CCDF) and PDF of R_j can be expressed as $\mathbb{P}(R_j>r)=\exp[\int_0^r -2\pi\lambda_j(r)r\mathrm{d}r]$ and $f_{R_j}(r)=2\pi\lambda_j(r)r\exp[-2\pi\int_0^r\lambda_j(r)r\mathrm{d}r]$.

Appendix B
Proof of (5)

With X_j being the minimum distance between the typical GUE and the j^{th} tier APs, the CCDF of the distance between the typical GUE and the k^{th} tier tagged AP X_k is given as

$$\begin{aligned}&\mathbb{P}(X_k>x)\\&=\frac{1}{A_k}\mathbb{P}\left[X_k>x,\bar{P}_{r,k}(X_k)>\max_{j,j\neq k}\bar{P}_{r,j}(X_j)\right]\\&=\frac{1}{A_k}\int_{\sqrt{x^2-H_k^2}}^{\infty}\prod_{\substack{j=1,\\ j\neq k}}^{5}\mathbb{P}\left[\bar{P}_{r,k}\left(\sqrt{r^2+H_k^2}\right)>\bar{P}_{r,j}\left(\sqrt{R_j^2+H_j^2}\right)\right]\\&\quad\times f_{R_k}(r)\mathrm{d}r\\&=\frac{2\pi}{A_k}\int_{\sqrt{x^2-H_k^2}}^{\infty}\lambda_k(r)r\exp\left[-2\pi\sum_{j=1}^{5}\int_0^{\widehat{r}_j}\lambda_j(r)r\mathrm{d}r\right]\mathrm{d}r.\end{aligned}\tag{35}$$

Based on the CCDF, we can obtain the PDF of X_k as shown in (5).

Appendix C
Proof of (7)

The PDF of the area C of a Poisson Voronoi cell is given by [40]

$$f_C(c)=\frac{3.5^{3.5}}{\Gamma(3.5)}c^{2.5}\exp(-3.5c).\tag{36}$$

Let $M_{k,0}$ denote the total number of GUEs associated with a k^{th} tier AP. For the MBS tier, i.e., $k=1$, the PMF of $M_{1,0}$ can be derived as

$$\begin{aligned}&\mathbb{P}(M_{1,0}=v)\\&=\int_0^{\infty}\mathbb{P}(\text{number of GUEs per MBS}=v|c)f_C(c)\mathrm{d}c\\&\overset{(a)}{=}\int_0^{\infty}\frac{\left(\frac{\lambda_{\mathrm{g}}A_1}{\lambda_{\mathrm{b}}}c\right)^v}{v!}\exp\left(-\frac{\lambda_{\mathrm{g}}A_1}{\lambda_{\mathrm{b}}}c\right)f_C(c)\mathrm{d}c\\&=\frac{3.5^{3.5}\left(\frac{\lambda_{\mathrm{g}}A_1}{\lambda_{\mathrm{b}}}\right)^v}{v!\Gamma(3.5)}\int_0^{\infty}c^{v+2.5}\exp\left[-\left(3.5+\frac{\lambda_{\mathrm{g}}A_1}{\lambda_{\mathrm{b}}}\right)c\right]\mathrm{d}c\\&\overset{(b)}{=}\frac{3.5^{3.5}\Gamma(v+3.5)\left(\frac{\lambda_{\mathrm{g}}A_1}{\lambda_{\mathrm{b}}}\right)^v}{v!\Gamma(3.5)\left(3.5+\frac{\lambda_{\mathrm{g}}A_1}{\lambda_{\mathrm{b}}}\right)^{v+3.5}}\end{aligned}\tag{37}$$

where equation (a) comes from the definition of PPP with mean $\frac{\lambda_{\mathrm{g}}A_1}{\lambda_{\mathrm{b}}}c$, which is the average number of GUEs in the association area c of an MBS, and equation (b) is derived from the definition of gamma function $\Gamma(x)=\int_0^{\infty}t^{x-1}e^{-t}\mathrm{d}t$. For the UAV tiers, because whether a UAV is in the 2^{nd} or 3^{rd} tier is independent of the number of GUEs associated with the UAV, we have $M_{2,0}=M_{3,0}$. The mean number of GUEs in the association area of a UAV is equal to $\frac{\lambda_{\mathrm{g}}(A_2+A_3)}{\lambda_{\mathrm{u}}}c$. Then, following the same derivation process, the PMFs of the total number of GUEs associated with a UAV or SBS can be found in (7) the same as (37).

Appendix D
Proof of (16) and (17)

The STP of a packet from the tagged AP to the typical GUE is given by

$$\begin{aligned}&\mathbb{P}(\gamma_{k,\mathbf{g}}^{(\mathrm{a})}>\tau_a)\\&=\mathbb{E}_{X_k}\left\{\mathbb{P}\left[h_{k,\mathbf{g}}>\tau_a P_{\mathrm{t},k}^{-1}\psi_{k,\mathrm{G}}^{-1}\zeta^{-1}x^{\alpha_k}\left(\sum_{j=1}^{5}I_j+\sigma_0B_0\right)\right]\right\}\end{aligned}\tag{38}$$

where $I_j=\sum_{\mathbf{x}_i\in\Phi_j\setminus\mathbf{x}^*}\delta_{j,i,\mathbf{g}}P_{\mathrm{t},j}h_{j,i,\mathbf{g}}\psi_{j,\mathrm{G}}^{(\mathrm{Int})}\zeta Y_{j,i}{}^{-\alpha_j}$ denotes the interference from the j^{th} tier APs to the typical GUE. Equation (38) can be further derived as

$$\begin{aligned}&\mathbb{P}\left(\gamma_{k,\mathbf{g}}^{(\mathrm{a})}>\tau_a\right)\\&\overset{(a)}{=}\mathbb{E}_{X_k}\mathbb{E}_I\left\{\frac{\Gamma\left[m_k,s_k\left(I+\sigma_0B_0\right)\right]}{\Gamma(m_k)}\right\}\\&\overset{(b)}{=}\mathbb{E}_{X_k}\mathbb{E}_I\left\{\exp\left[-s_k\left(I+\sigma_0B_0\right)\right]\sum_{c=0}^{m_k-1}\frac{\left[s_k\left(I+\sigma_0B_0\right)\right]^c}{c!}\right\}\\&\overset{(c)}{=}\mathbb{E}_{X_k}\left\{\sum_{c=0}^{m_k-1}(-1)^c\frac{s_k^c}{c!}\mathbb{E}_I\left\{\frac{\mathrm{d}^c\exp\left[-s_k(I+\sigma_0B_0)\right]}{\mathrm{d}s_k^c}\right\}\right\}\\&\overset{(d)}{=}\mathbb{E}_{X_k}\left[\sum_{c=0}^{m_k-1}\frac{s_k^c}{c!}\exp(-s_k\sigma_0B_0)\sum_{d=0}^{c}(-1)^{2c-d}C_c^d\sigma_0{}^{c-d}\cdot\right.\\&\qquad\left.B_0{}^{c-d}\frac{\mathrm{d}^d\mathcal{L}_I\left(s_k\right)}{\mathrm{d}s_k^d}\right]\end{aligned}\tag{39}$$

where $I=\sum_{j=1}^{5}I_j$, $s_k=\frac{m_k\tau_a}{P_{\mathrm{t},k}\psi_{k,G}\zeta x^{-\alpha_k}}$. Equation (a) comes from the gamma distribution of $h_{k,\mathbf{g}}$; equation (b) comes from the expressions of the gamma function and the upper incomplete gamma function; equation (c) is derived from $\exp[-s_k(I+\sigma_0B_0)](I+\sigma_0B_0)^c=(-1)^c\frac{\mathrm{d}^c\exp[-s_k(I+\sigma_0B_0)]}{\mathrm{d}s_k^c}$; and equation (d) comes from the Leibniz integral formula and the binomial expansion. The Laplace transform in (39) can be expressed as

$$\begin{aligned}&\mathcal{L}_I\left(s_k\right)\\&=\mathbb{E}_I\left[\exp\left(-s_kI\right)\right]\end{aligned}$$

$$= \prod_{j=1}^{5} \mathbb{E}_{\Phi_j} \left[\prod_{\mathbf{x}_i \in \Phi_j} \exp\left(-s_k \delta_{j,i,\mathbf{g}} P_{\mathrm{t},j} h_{j,i,\mathbf{g}} \psi_{j,\mathrm{G}}^{(\mathrm{Int})} \zeta Y_{j,i}^{-\alpha_j} \right) \right]$$

$$\overset{(a)}{=} \prod_{j=1}^{5} \exp\left\{ -\mathbb{P}(\delta_{j,i,\mathbf{g}} = 1) \frac{\int_0^\infty \lambda_j(r) r \mathrm{d}r}{\int_0^\infty r \mathrm{d}r} \cdot \int_S \left\{ 1 - \mathbb{E}_{h_{j,i,\mathbf{g}}} \left[\exp\left(-s_k P_{\mathrm{t},j} h_{j,i,\mathbf{g}} \psi_{j,\mathrm{G}}^{(\mathrm{Int})} \zeta Y_{j,i}^{-\alpha_j} \right) \right] \right\} \mathrm{d}\mathbf{x}_i \right\}$$

$$\overset{(b)}{=} \prod_{j=1}^{5} \exp\left\{ -2\pi \mathbb{P}(\delta_{j,i,\mathbf{g}} = 1) \frac{\int_0^\infty \lambda_j(r) r \mathrm{d}r}{\int_0^\infty r \mathrm{d}r} \left\{ \int_{y_{\min}}^{\infty} y \mathrm{d}y - \mathbb{E}_{\psi_{j,\mathrm{G}}^{(\mathrm{Int})}} \left[\int_{y_{\min}}^{\infty} \left(\frac{m_j}{s_k P_{\mathrm{t},j} \psi_{j,\mathrm{G}}^{(\mathrm{Int})} \zeta y^{-\alpha_j} + m_j} \right)^{m_j} y \mathrm{d}y \right] \right\} \right\} \tag{40}$$

where $y_{\min} = \left(\frac{T_j}{T_k}\right)^{\frac{1}{\alpha_j}} x^{\frac{\alpha_k}{\alpha_j}}$, equation (a) comes from the probability generating functional of PPP, and equation (b) holds as $h_{j,i,\mathbf{g}}$ is gamma distributed. The integral in (40) can be further derived as

$$\int_{y_{\min}}^{\infty} \left(\frac{m_j}{s_k P_{\mathrm{t},j} \psi_{j,\mathrm{G}}^{(\mathrm{Int})} \zeta y^{-\alpha_j} + m_j} \right)^{m_j} y \mathrm{d}y$$

$$\overset{w = y^{\alpha_j}}{=} \frac{1}{\alpha_j} \int_{y_{\min}^{\alpha_j}}^{\infty} \left[1 - \frac{1}{1 + m_j \left(P_{\mathrm{t},j} \psi_{j,\mathrm{G}}^{(\mathrm{Int})} \zeta s_k \right)^{-1} w} \right]^{m_j} w^{\frac{2}{\alpha_j} - 1} \mathrm{d}w$$

$$\overset{(a)}{=} \frac{1}{\alpha_j} \int_{y_{\min}^{\alpha_j}}^{\infty} \sum_{t=0}^{m_j} C_{m_j}^t (-1)^t \frac{w^{\frac{2}{\alpha_j} - 1}}{\left[1 + m_j \left(P_{\mathrm{t},j} \psi_{j,\mathrm{G}}^{(\mathrm{Int})} \zeta s_k \right)^{-1} w \right]^t} \mathrm{d}w$$

$$\overset{(b)}{=} \int_{y_{\min}}^{\infty} y \mathrm{d}y + \frac{1}{\alpha_j} \sum_{t=1}^{m_j} C_{m_j}^t (-1)^t \frac{y_{\min}^{2 - \alpha_j t} \left(P_{\mathrm{t},j} \psi_{j,\mathrm{G}}^{(\mathrm{Int})} \zeta s_k \right)^t}{\left(t - \frac{2}{\alpha_j} \right) m_j^t} \cdot {}_2F_1\left(t, t - \frac{2}{\alpha_j}; t - \frac{2}{\alpha_j} + 1; -\frac{P_{\mathrm{t},j} \psi_{j,\mathrm{G}}^{(\mathrm{Int})} \zeta s_k}{m_j y_{\min}^{\alpha_j}} \right) \tag{41}$$

where equation (a) comes from the binomial expansion, equation (b) comes from using [41] [Eq. 3.194.2], and ${}_2F_1()$ is the Gaussian hypergeometric function. Combining (38)–(41), we obtain the STP of a packet from the k^{th} tier AP to the typical GUE by (16).

Appendix E
Proof of (18)

Since the packet service process over an access link of an interfering AP is the same as that of the tagged AP, we adopt the same Geom/Geom/1 queueing model to analyze the packet transmissions from an interfering AP to its associated GUEs. Assume that a j^{th} tier interfering AP is associated with M_j GUEs. Then, the average number of active GUEs associated with the interfering AP is $M_j \left[1 - Q_{j,M_j}^{(\mathrm{a})}(0) \right]$, where $Q_{j,M_j}^{(\mathrm{a})}(0)$ is the steady-state probability given the same as (14) by

$$Q_{j,M_j}^{(\mathrm{a})}(0) = 1 - \xi / \mu_{j,M_j}^{(\mathrm{a})}, \; M_j = 0, 1, \ldots, M_{j,\max}. \tag{42}$$

Here, $\mu_{j,M_j}^{(\mathrm{a})}$ is the packet service probability of the interfering AP for an associated GUE, which depends on the subchannel contention and STP. Due to the same analysis and derivation process, we can obtain $\mu_{j,M_j}^{(\mathrm{a})}$ similar to $\mu_{k,M_k}^{(\mathrm{a})}$ in (15).

If the number of active associated GUEs is less than the number of access subchannels $F^{(\mathrm{a})}$, then the interfering AP has packet(s) to send on the same subchannel allocated to the typical GUE $\mathbf{g}$ with probability $\frac{M_j \left[1 - Q_{j,M_j}^{(\mathrm{a})}(0) \right]}{F^{(\mathrm{a})}}$. Otherwise, the probability is 1. Thus, the probability that the i^{th} interfering AP in the j^{th} tier has packet(s) to send on the same subchannel allocated to $\mathbf{g}$ is

$$\mathbb{P}(\delta_{j,i,\mathbf{g}} = 1) = \sum_{v'=1}^{M_{j,\max}} \min\left\{ \frac{v' \xi}{\mu_{j,v'}^{(\mathrm{a})} F^{(\mathrm{a})}}, 1 \right\} \cdot \mathbb{P}(M_j = v'). \tag{43}$$

Appendix F
Proof of (20)

The packet service probability on a subchannel of the backhaul link from the serving MBS to the tagged IAB node is given by

$$\mu_{\mathrm{I}}^{(\mathrm{b})} = \mathbb{E}_{Z_{\mathrm{I}}} \left[\mathbb{P}(\gamma_{\mathrm{I}}^{(\mathrm{b})} > \tau_b) \right]$$

$$\overset{(a)}{=} \mathbb{E}_{Z_{\mathrm{I}}} \left[\frac{\Gamma(m_{\mathrm{I}}, \frac{m_{\mathrm{I}} \tau_b \sigma_0 B_0}{P_{\mathrm{t},1} \psi_{\mathrm{B},\mathrm{I}} \zeta z^{-\alpha_{\mathrm{I}}}})}{\Gamma(m_{\mathrm{I}})} \right]$$

$$= \mathbb{E}_{Z_{\mathrm{I}}} \left[\exp\left(-\frac{m_{\mathrm{I}} \tau_b \sigma_0 B_0}{P_{\mathrm{t},1} \psi_{\mathrm{B},\mathrm{I}} \zeta z^{-\alpha_{\mathrm{I}}}} \right) \sum_{c=0}^{m_{\mathrm{I}}-1} \frac{\left(\frac{m_{\mathrm{I}} \tau_b \sigma_0 B_0}{P_{\mathrm{t},1} \psi_{\mathrm{B},\mathrm{I}} \zeta z^{-\alpha_{\mathrm{I}}}} \right)^c}{c!} \right]$$

$$= \int_{\Delta H_{\mathrm{I}}}^{\infty} \exp\left(\frac{-m_{\mathrm{I}} \tau_b \sigma_0 B_0}{P_{\mathrm{t},1} \psi_{\mathrm{B},\mathrm{I}} \zeta z^{-\alpha_{\mathrm{I}}}} \right) \sum_{c=0}^{m_{\mathrm{I}}-1} \frac{\left(\frac{m_{\mathrm{I}} \tau_b \sigma_0 B_0}{P_{\mathrm{t},1} \psi_{\mathrm{B},\mathrm{I}} \zeta z^{-\alpha_{\mathrm{I}}}} \right)^c}{c!} \cdot 2\pi \lambda_{\mathrm{b}} z \exp\left[-\pi \lambda_{\mathrm{b}} (z^2 - \Delta H_{\mathrm{I}}^2) \right] \mathrm{d}z \tag{44}$$

where (a) comes from the gamma distribution of $h_{\mathrm{B,I}}$.

References

[1] Y. Zhang et al., "Throughput analysis of UAV-assisted IAB cellular networks with heterogeneous traffic," in *Proc. IEEE Wirel. Commun. Netw. Conf.*, 2022, pp. 902–907.

[2] M. Xiao et al., "Millimeter wave communications for future mobile networks," *IEEE J. Sel. Areas Commun.*, vol. 35, no. 9, pp. 1909–1935, Sep. 2017.

[3] X. Wang et al., "Millimeter wave communication: A comprehensive survey," *IEEE Commun. Surv. Tutor.*, vol. 20, no. 3, pp. 1616–1653, thirdquarter, 2018.

[4] H. Wu, X. Tao, N. Zhang, and X. Shen, "Cooperative UAV cluster-assisted terrestrial cellular networks for ubiquitous coverage," *IEEE J. Sel. Areas Commun.*, vol. 36, no. 9, pp. 2045–2058, Sep. 2018.

[5] S. Fu et al., "Joint unmanned aerial vehicle (UAV) deployment and power control for Internet of Things networks," *IEEE Trans. Veh. Technol.*, vol. 69, no. 4, pp. 4367–4378, Apr. 2020.

[6] N. Zhao et al., "UAV-assisted emergency networks in disasters," *IEEE Wirel. Commun.*, vol. 26, no. 1, pp. 45–51, Feb. 2019.

[7] S. Zhu, L. Gui, N. Cheng, F. Sun, and Q. Zhang, "Joint design of access point selection and path planning for UAV-assisted cellular networks," *IEEE Internet Things J.*, vol. 7, no. 1, pp. 220–233, Jan. 2020.
[8] M. Li et al., "Energy-efficient UAV-assisted mobile edge computing: Resource allocation and trajectory optimization," *IEEE Trans. Veh. Technol.*, vol. 69, no. 3, pp. 3424–3438, Mar. 2020.
[9] G. Zhang, T. Q. S. Quek, M. Kountouris, A. Huang, and H. Shan, "Fundamentals of heterogeneous backhaul design analysis and optimization," *IEEE Trans. Commun.*, vol. 64, no. 2, pp. 876–889, Feb. 2016.
[10] "NR; Study on integrated access and backhaul," 3rd Generation Partnership Project, Sophia Antipolis, France, Tech. Rep. 38.874 (Rel. 16), Dec. 2018.
[11] C. Saha et al., "Bandwidth partitioning and downlink analysis in millimeter wave integrated access and backhaul for 5G," *IEEE Trans. Wireless Commun.*, vol. 17, no. 12, pp. 8195–8210, Dec. 2018.
[12] C. Saha and H. S. Dhillon, "Millimeter wave integrated access and backhaul in 5G: Performance analysis and design insights," *IEEE J. Sel. Areas Commun.*, vol. 37, no. 12, pp. 2669–2684, Dec. 2019.
[13] M. Gapeyenko et al., "Flexible and reliable UAV-assisted backhaul operation in 5G mmWave cellular networks," *IEEE J. Sel. Areas Commun.*, vol. 36, no. 11, pp. 2486–2496, Nov. 2018.
[14] N. Tafintsev et al., "Aerial access and backhaul in mmwave B5G systems: Performance dynamics and optimization," *IEEE Commun. Mag.*, vol. 58, no. 2, pp. 93–99, Feb. 2020.
[15] D. López-Pérez et al., "A survey on 5G radio access network energy efficiency: Massive MIMO, lean carrier design, sleep modes, and machine learning," *IEEE Commun. Surv. Tutor.*, vol. 24, no. 1, pp. 653–697, Firstquarter, 2022.
[16] S. Buzzi et al., "A survey of energy-efficient techniques for 5G networks and challenges ahead," *IEEE J. Sel. Areas Commun.*, vol. 34, no. 4, pp. 697–709, Apr. 2016.
[17] Y. Zeng, Q. Wu, and R. Zhang, "Accessing from the sky: A tutorial on UAV communications for 5G and beyond," *Proc. IEEE*, vol. 107, no. 12, pp. 2327–2375, Dec. 2019.
[18] M. Mozaffari, W. Saad, M. Bennis, Y.-H. Nam, and M. Debbah, "A tutorial on UAVs for wireless networks: Applications, challenges, and open problems," *IEEE Commun. Surv. Tutor.*, vol. 21, no. 3, pp. 2334–2360, thirdquarter, 2019.
[19] Y. Li and L. Cai, "UAV-assisted dynamic coverage in a heterogeneous cellular system," *IEEE Netw.*, vol. 31, no. 4, pp. 56–61, Jul. 2017.
[20] J. Chakareski et al., "An energy efficient framework for UAV-assisted millimeter wave 5G heterogeneous cellular networks," *IEEE Trans. Green Commun. Netw.*, vol. 3, no. 1, pp. 37–44, Mar. 2019.
[21] S. Lagen, A. Agustin, and J. Vidal, "Decentralized coordinated precoding for dense TDD small cell networks," *IEEE Trans. Wireless Commun.*, vol. 14, no. 8, pp. 4546–4561, Aug. 2015.
[22] Q. Zhang, H. H. Yang, T. Q. S. Quek, and S. Jin, "Spatiotemporal modeling of massive MIMO systems with mixed-type IoT devices: Scheduling optimization with delay constraints," *IEEE Internet Things J.*, vol. 8, no. 12, pp. 10146–10159, Jun. 2021.
[23] Y. Wang, H. H. Yang, Q. Zhu, and T. Q. S. Quek, "Analysis of packet throughput in spatiotemporal HetNets with scheduling and various traffic loads," *IEEE Wireless Commun. Lett.*, vol. 9, no. 1, pp. 95–98, Jan. 2020.
[24] J. Li et al., "Analysis of packet throughput in small cell networks under clustered dynamic TDD," *IEEE Trans. Wireless Commun.*, vol. 17, no. 9, pp. 5729–5742, Sep. 2018.
[25] M. Song et al., "Joint optimization of fractional frequency reuse and cell clustering for dynamic TDD small cell networks," *IEEE Trans. Wireless Commun.*, vol. 21, no. 1, pp. 398–412, Jan. 2022.
[26] S. Ahmed, M. Z. Chowdhury, and Y. M. Jang, "Energy-efficient UAV-to-user scheduling to maximize throughput in wireless networks," *IEEE Access*, vol. 8, pp. 21215–21225, 2020.
[27] L. Liu, A. Wang, G. Sun, and J. Li, "Multiobjective optimization for improving throughput and energy efficiency in UAV-enabled IoT," *IEEE Internet Things J.*, vol. 9, no. 20, pp. 20763–20777, Oct. 2022.
[28] S. Aboagye, A. Ibrahim, and T. M. N. Ngatched, "Frameworks for energy efficiency maximization in HetNets with millimeter wave backhaul links," *IEEE Trans. Green Commun. Netw.*, vol. 4, no. 1, pp. 83–94, Mar. 2020.
[29] A. Masaracchia et al., "Energy-efficient and throughput fair resource allocation for TS-NOMA UAV-assisted communications," *IEEE Trans. Commun.*, vol. 68, no. 11, pp. 7156–7169, Nov. 2020.
[30] X. Lin, G. Su, B. Chen, H. Wang, and M. Dai, "Striking a balance between system throughput and energy efficiency for UAV-IoT systems," *IEEE Internet Things J.*, vol. 6, no. 6, pp. 10519–10533, Dec. 2019.
[31] S. Sadr and R. S. Adve, "Handoff rate and coverage analysis in multi-tier heterogeneous networks," *IEEE Trans. Wireless Commun.*, vol. 14, no. 5, pp. 2626–2638, May 2015.
[32] A. Al-Hourani, S. Kandeepan, and S. Lardner, "Optimal LAP altitude for maximum coverage," *IEEE Wirel. Commun. Lett.*, vol. 3, no. 6, pp. 569–572, Dec. 2014.
[33] T. Bai, R. Vaze, and R. W. Heath, "Analysis of blockage effects on urban cellular networks," *IEEE Trans. Wireless Commun.*, vol. 13, no. 9, pp. 5070–5083, Sep. 2014.
[34] N. Kouzayha et al., "Analysis of large scale aerial terrestrial networks with mmWave backhauling," *IEEE Trans. Wireless Commun.*, vol. 20, no. 12, pp. 8362–8380, Dec. 2021.
[35] D. Kim, J. Lee, and T. Q. S. Quek, "Multi-layer unmanned aerial vehicle networks: Modeling and performance analysis," *IEEE Trans. Wireless Commun.*, vol. 19, no. 1, pp. 325–339, Jan. 2020.
[36] W. Wu et al., "Fast mmwave beam alignment via correlated bandit learning," *IEEE Trans. Wirel. Commun.*, vol. 18, no. 12, pp. 5894–5908, Dec. 2019.
[37] A. S. Alfa, *Applied Discrete-Time Queues*. Berlin, Germany:Springer2016.
[38] Y. Zhong, T. Q. S. Quek, and X. Ge, "Heterogeneous cellular networks with spatio-temporal traffic: Delay analysis and scheduling," *IEEE J. Sel. Areas Commun.*, vol. 35, no. 6, pp. 1373–1386, Jun. 2017.
[39] A. Aubry, A. D. Maio, A. Zappone, M. Razaviyayn, and Z.-Q. Luo, "A new sequential optimization procedure and its applications to resource allocation for wireless systems," *IEEE Trans. Signal Process.*, vol. 66, no. 24, pp. 6518–6533, Dec. 2018.
[40] J.-S. Ferenc et al., "On the size distribution of poisson voronoi cells," *Physica A., Statist. Mech. Appl.*, vol. 385, no. 2, pp. 518–526, Nov. 2007.
[41] I. S. Gradshteyn and I. Ryzhik, "Table of integrals, series, and products," *Math Comput.*, vol. 20, no. 96, pp. 1157–1160, 2007.

Yue Zhang received the B.Eng. degree in communication engineering from Nanchang University, Nanchang, China, in 2020. She is currently working twoard the Ph.D. degree with the Institute of Information and Communication Network Engineering, Zhejiang University, Hangzhou, China. Her research interests include the design and optimization of the UAV-assisted cellular networks and integrated sensing and communication networks.

Hangguan Shan (Senior Member, IEEE) received the B.Sc. degree in electrical engineering from Zhejiang University, Hangzhou, China, in 2004, and the Ph.D. degree in electrical engineering from Fudan University, Shanghai, China, in 2009. From 2009 to 2010, he was a Postdoctoral Research Fellow at the University of Waterloo, Waterloo, ON, Canada. Since 2011, he has been with the College of Information Science and Electronic Engineering, Zhejiang University, where he is currently an Associate Professor. He is also with the Zhejiang Provincial Key Laboratory of Information Processing and Communication Networks, Zhejiang University, and SUTD-ZJU IDEA, Zhejiang University. His research interests include machine learning-enabled resource allocation and quality-of-service provisioning in wireless networks. Dr. Shan was the recipient of the Best Industry Paper Award from the 2011 IEEE WCNC held in Quintana Roo, Mexico. He was the Technical Program Committee Member of various international conferences. He was the Editor of the IEEE TRANSACTIONS ON GREEN COMMUNICATIONS AND NETWORKING.

Meiyan Song received the B.Eng. degree in communication engineering from the Wuhan University of Technology, Wuhan, China, in 2018. She is currently working toward the Ph.D. degree with the Institute of Information and Communication Engineering, Zhejiang University, Hangzhou, China. Her research interests include the analysis of heterogeneous cellular networks using tools from stochastic geometry and queuing theory.

Howard H. Yang (Member, IEEE) received the B.E. degree in communication engineering from the Harbin Institute of Technology, Harbin, China, in 2012, and the M.Sc. degree in electronic engineering from the Hong Kong University of Science and Technology, Hong Kong, in 2013, and the Ph.D. degree in electrical engineering from the Singapore University of Technology and Design (SUTD), Singapore, in 2017. He was a Postdoctoral Research Fellow at SUTD from 2017 to 2020, a Visiting Postdoc Researcher with Princeton University, Princeton, NJ, USA, from 2018 to 2019, and a Visiting Student at the University of Texas at Austin, Austin, TX, USA, from 2015 to 2016. He is currently an Assistant Professor with the Zhejiang University, Hangzhou, China, University of Illinois at Urbana-Champaign Institute, Champaign, IL, USA, Zhejiang University. He is also an Adjunct Assistant Professor with the Department of Electrical and Computer Engineering, University of Illinois Urbana-Champaign. His research interests include various aspects of wireless communications, networking, and signal processing, currently focusing on the modeling of modern wireless networks, high dimensional statistics, graph signal processing, and machine learning. He is the Editor of the IEEE TRANSACTIONS ON WIRELESS COMMUNICATIONS. He was the recipient of the IEEE Signal Processing Society Best Paper Award in 2022, the IEEE WCSP ten Year Anniversary Excellent Paper Award in 2019, and the IEEE WCSP Best Paper Award in 2014.

Xuemin (Sherman) Shen (Fellow, IEEE) received the Ph.D. degree in electrical engineering from Rutgers University, New Brunswick, NJ, USA, in 1990. He is currently a University Professor with the Department of Electrical and Computer Engineering, University of Waterloo, Waterloo, ON, Canada. His research interests include network resource management, wireless network security, Internet of Things, 5G and beyond, and vehicular ad hoc and sensor networks. Dr. Shen is a Registered Professional Engineer of Ontario, Canada, an Engineering Institute of Canada Fellow, Canadian Academy of Engineering Fellow, Royal Society of Canada Fellow, Chinese Academy of Engineering Foreign Member, and Distinguished Lecturer of the IEEE Vehicular Technology Society and Communications Society. Dr. Shen was the recipient of the Canadian Award for Telecommunications Research from the Canadian Society of Information Theory in 2021, R.A. Fessenden Award in 2019 from IEEE, Canada, Award of Merit from the Federation of Chinese Canadian Professionals (Ontario) in 2019, James Evans Avant Garde Award in 2018 from the IEEE Vehicular Technology Society, Joseph LoCicero Award in 2015 and Education Award in 2017 from the IEEE Communications Society, and Technical Recognition Award from Wireless Communications Technical Committee (2019) and AHSN Technical Committee (2013). He was also the recipient of the Excellent Graduate Supervision Award in 2006 from the University of Waterloo and the Premier's Research Excellence Award (PREA) in 2003 from the Province of Ontario, Canada. He was the Technical Program Committee Chair/CoChair for IEEE Globecom'16, IEEE Infocom'14, IEEE VTC'10 Fall, IEEE Globecom'07, and the Chair for the IEEE Communications Society Technical Committee on Wireless Communications. Dr. Shen is the President of the IEEE Communications Society. He was the Vice President for Technical & Educational Activities, Vice President for Publications, Member-at-Large on the Board of Governors, Chair of the Distinguished Lecturer Selection Committee, Member of IEEE Fellow Selection Committee of the ComSoc. Dr. Shen was the Editor-in-Chief of the IEEE INTERNET OF THINGS JOURNAL, IEEE NETWORK, and *IET Communications*.

Qi Zhang received the B.Sc. degree in computer science from Zhejiang University, Hangzhou, China, in 1999, and the EMBA degree from the joint EMBA program of Ecole Nationale des Ponts et Chaussées and Tongji University, Shanghai, China, in 2010. He has more than 20 years of experience in internet and telecommunication domain. Since 2002 he has been with Nokia in various technical positions, and R&D leadership and business leadership positions. He is currently the Executive Vice President of Nokia Shanghai Bell, Head of Nokia Mobile Network China. He has been leading the TD-LTE business line since 2013, and has successfully accelerated product roadmap and won business, not only in China but also around world. His research interests include the evolution of mobile communication networks, AI, intelligent throughput efficiency, energy saving and carbon reduction technologies and solutions in wireless networks. He has been awarded as one of the Top ten 5G industry leaders of China in 2018. He was the technical committee member of various national science and technology associates.

Xianhua He received the Master degree in system engineering from Southeast University, Nanjing, China, in 2004. He has more than twenty years of experience in internet and telecommunication domain designing wireless communication system products, including PHS, 4G, and 5G. He has held various positions such as Software Architect, Chief Innovation Architect, System Architect, Senior Technical Manager, and Senior Manager of radio access network architecture and specification team. From 2002 to 2005, he was a Senior Software Engineer with UTStarcom Co. Ltd. Since 2006, he has been with Nokia in Hangzhou, China and was recognized as a Distinguished Member of the Technical Staff by Nokia Bell Labs in 2020. His research interests include radio resource management, AI, IoT, energy saving and V2X solutions in wireless networks.